Faculty of Graduate Studies

Chemistry Department

Graphene Oxide Nanoparticles for Treatment of Toxic Nickel Ions from Water

By:

Majdoleen Mohammad Alatawna

Supervisor:

Dr. Sami Makharza

Co-supervisor:

Dr. Fahed Takrori

This Thesis Submitted in Partial Fulfillment of the Requirements for the Degree of Master of Chemistry, College of Graduate Studies & Academic Research, Hebron University, Palestine.

2020

Committee Decision

We, the undersigned, approve the Master's Thesis of Majdoleen Alatawna.

Thesis Title: Graphene Oxide Nanoparticles for Treatment of Toxic Nickel Ions from Water.

This thesis was successfully defended on December, 2020 and approved by:

Committee members		Signature
Supervisor	Dr. Sami Makharza	
Co-supervisor	Dr. Fahed Takrori	
Internal examiner	Dr. Nader Yaghi	
External examiner	Dr.Rasha Ghunaim	
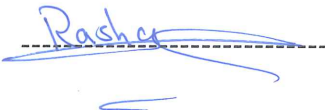
Dedication

My years at the University of Hebron as a graduate student wouldn't have been as great without the support and encouragement of people around me during the entire journey. My sincere thanks are due to them for making me able to finish this thesis. No word can describe my appreciation and gratitude, and so I dedicate this thesis to them.

*Without the support of my family, I would be nowhere. "Thank you" is an abbreviation of what they have done and are still doing for me. I would like to thank my parents, **Dad and Mom**, for constantly pushing me to try to be better, and for encouraging me to pursue a Master's degree. I would also like to thank my brothers and my sisters for everything!*

*I also dedicate this work to my Consultant, **Dr. Sami Makharza**. I wouldn't have graduated now had it not been for his patience and belief in me.*

*Finally, special thanks to my colleagues **Sahar Zahran**, **Rasheda Abu-Hamdia,** and **Razan Hroub** for their support during my research period which gave me the passion to complete this thesis successfully.*

Acknowledgment

I would like to express my sincere gratitude to my advisor, **_Dr. Sami- Makharza,_** for all of his support and guidance throughout the research. My thanks are also due to my co-supervisor, **_Dr. Fahd Takrori_**.

I would like to thank the faculty and staff in the chemistry department at Hebron University for their support and assistance. I also would like to extend my thanks to the lab technicians at the faculty of pharmacy and medical science.

Table of contents

List of Tables

List of Figures

List of Scheme

List of Abbreviations

CAA	Commercial activated alumina
CAC	Commercial activated carbon
C_e	Concentration at equilibrium (ppm)
C_i	Initial concentration (ppm)
CNF	Carbon nanofiber
CNT	Carbon nanotubes
GO	Graphene oxide
FT-IR	Fourier-transform infrared spectroscopy
K_D	Distribution coefficient
K_f	Freundlich constant related to the adsorption capacity
K_L	Langmuir constant (L/mg)
K_1	Pseudo-first-order rate constant (min^{-1})
K_2	Pseudo-second-order rate constant (g/mg.min)
MWCNT	Multi wall carbon nanotube
m	Mass (g)
n	Freundlich constant related to the adsorption intensity
q_e	Adsorption capacity at equilibrium (mg/g)
$q_{e.cal}$	Adsorption capacity at equilibrium, calculated
$q_{e.exp}$	Adsorption capacity at equilibrium, experimental
q_m	Maximum adsorption capacity (mg/g)
q_t	Adsorption capacity at time (mg/g)
R	Ideal gas constant 8.314(J.mol/K)
R^2	Regression coefficient
SEM	Scanning electron microscope
SDS	Sodium dodecyl sulphate
SWCNT	Single wall carbon nanotube
T	Temperature (°C)
t	Time (min)
UV-vis	Ultra violet-visible spectroscopy
V	Volume
%R	Percentage removal
ΔG	Gibbes free energy (KJ/mol)
ΔH	Enthalpy change (KJ/mol)
ΔS	Entropy (J/mol.K)

Abstract

This study investigated the removal of nickel (II) ions by using two sizes of graphene oxide nanoparticles (GO-450 nm and GO-200 nm). The thickness and lateral sheet dimensions of GO are considered to be an important adsorbent and promising method for sufficient removal of metals like nickel, lead, copper, etc. The graphite oxide was prepared by oxidation-reduction reaction (Hummers method), and the final product was labeled GO – 450 nm. A tip sonicator was used to reduce the size particles to 200 nm under controlled conditions (time and power of sonication). FTIR spectroscopy shows that both sizes of GO particles contain several types of oxygen groups distributed onto the surface of GO particles. Scanning electron microscopy (SEM) and the statistical analysis confirmed the formation of these two sizes of GO particles. The GO – 200 nm performed better removal of Ni (II) comparing with GO – 450 nm, due to more surfaces are available. The adsorption capacity of GO particles increased drastically from 45 mg/g to 75 mg/g for GO – 450 nm and GO – 200 nm respectively, these values were carried out after 2 h of incubation. The kinetics of adsorption and several parameters like initial concentration at equilibrium, pH, temperature, and adsorbent dose are controlled and studied by using UV-visible spectroscopy. The results indicated a significant potential of the GO – 200 nm as an adsorbent for Ni (II) ion removal.

Chapter One:

Introduction

1.1 Nanoscience and Nanotechnology

In 1959, on the occasion of the meeting of the American Physical Society, Physics Nobel laureate Richard Feynman gave a talk at the California Institute of Technology. The talk was entitled 'There's Plenty of Room at the Bottom'.Although Feynman was unable to predict this, this lecture was to become a central point in the nanotechnology field long before anything related to the word nano emerged [1]. The term (nano) derives from the Greek word for "dwarf". Hence, a nanometer (nm) is one-billionth of a meter. Nanotechnology is that the understanding and control of matter at dimensions of roughly 1-100 nm, approximately 100,000 times smaller than the diameter of a human hair [2].

 The nanometer-scale is commonly indicated as 1–100 nm, however nanoscience and nanotechnology often deal with objects bigger than 100 nm [2, 3]. Figure.1 shows the comparison of nanomaterials with large sized materials. Jumping from the scale of normal microscopy, (a millionth of a meter), to the nanoscale, (a billionth of a meter), has required the development of new techniques and modern instruments to observe and assemble molecules [1].

A nanomaterial has unique optical, magnetic, electrical, and other emergent properties. Thus all of these properties have given nanomaterials great impacts in all areas of our life [3]. Once concerning nanoscale material could be a combination of chemistry and physics occur chiefly to develop novel properties of matter [4]. Furthermore this scale, materials often has some new size-based properties such as high surface area, particle propagation distance, more adsorption sites, compressible without reducing surface area, high reactivity; some of them are superparamagnetic [5].
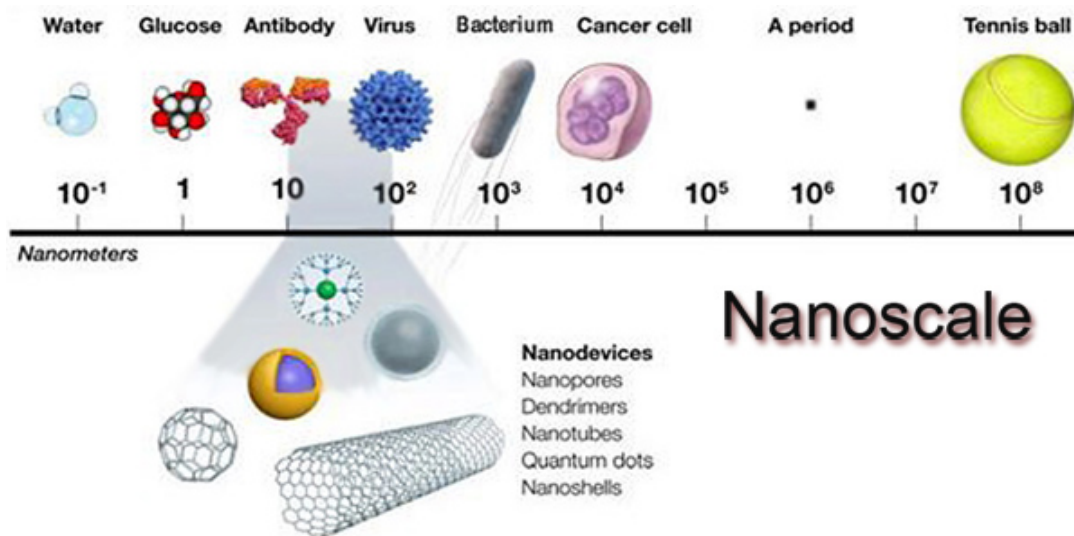
Figure 1. *A size comparison of nanoparticles with other larger-sized materials.* [3].

Therefore it suggests that nanotechnology holds the promise of tremendous improvements in manufacturing technologies, electronics, communications, health, and even environmental processing. For example, promising applications of nanotechnology in medicine and/ or biology have attracted a lot of attention and have become a fast-growing field. One of the attractive applications in nanomedicine is the creation of nanoscale devices for improved therapy and diagnostics. While the range of application areas of nanotechnology include in microelectronics for circuits, sensors, displays, data storage materials of all kinds for paints, coatings (including sun-tans), energy applications for solar cells, fuel cells, etc., in environmental applications and scientific instrumentation of various kinds, including many concerned with chemical analysis [6, 7]. Therefore nanotechnology considers the technology of the 21st century. And it is known to be a boon to humanity. It has made tremendous progress in recent decades [1].

1.2 Water Pollution and Water Pollutants

It is clear in our minds that water is the sign of life and is an important resource since life depends on it, and it is important for a variety of activities, such as agriculture, industries, households, recreation, and the environment [8]. It is important to remember that only 2.5% of the earth's water is fresh, and about 90% of it is locked up in polar ice caps and deep groundwater reservoirs [9]. However, part of bio-available water is polluted due to human activities.

Water pollution are projected to escalate in the coming decades, due to the effects of growing industrialization and urbanization, population growth, pollution, and climate change [10, 11]. With the increasing population in the world, the challenge of providing clean and fresh water is growing rapidly, causing major health problems [12].

Chemical pollutants have two sub-categories; inorganic pollutants including elements as heavy metals(arsenic, chromium, lead etc.,)and inorganic compound such as salt of cyanide, asbestos etc., The other type of chemical pollutants is organic compound as polycyclic aromatic hydrocarbons (PAHs), polychlorinated biphenyls (PCBs) etc., Chemical pollutants either organic or inorganic are the most important types among the other water pollutants, since it has the most negative impacts to biosphere and most of them are classified as a group one carcinogen such as arsenic and arsenic compounds, nickel compounds, aflatoxin, cadmium and cadmium compounds, asbestos , benzene etc., [13].

Heavy metals have relatively more important among other aquatic pollutants, given their persistence, bio-magnification, and toxicity. Heavy metals can enter the food chain easily through a number of pathways and cause progressive toxic effects in living organisms over their life span with gradual accumulation. Therefore an efficient methods and techniques

4

are required to enhance the efficiency of heavy metal removal from water and in turn, enhanced the quality of water [4, 14].

1.3 Heavy Metal Properties and their Environmental Effects

Several definition are put to explain the term of heavy metals including that elements with atomic weights of 63.5 to 200.6 g/mol other definition is; metals and metalloids with an atomic density greater than 4 g/cm^3 or at least 5 times greater than that of specific gravity of water [15], but has also been used for other metals. A recent IUPAC Technical Report (Duffus, 2002) discusses the inappropriateness of this term and the term is avoided. Thus, the most acceptably definition is that describe the term of heavy metal is but by *Robert Goyer* in his report that submitted *U.S. environmental protection agency in2004,* who define the heavy metal according to their impact to biosphere, especially to human health [16].

Heavy metals are natural constituents of the Earth's crust and exist in colloidal, particulate and dissolved phases in surface waters. The colloidal and particulate metal can be found as hydroxides, oxides, oxyanions, silicates, sulfides, or bond adsorbed to silicate clay, and organic matter [17].

Heavy metals are substantial pollutants to the environment. Heavy metals are released to the aquatic environment through various sources include, the paper industry, microelectronics, mining, nuclear power plants, battery manufacturing industries, etc.,.[18].

The solubility of heavy metals is relatively high; therefore, aquatic biota can absorb large quantity of soluble heavy metals. Moreover, in contrast to organic pollutants, heavy metals are not biodegradable and tend to be accumulated in living organism's tissues [15].

High concentrations of heavy metals can be accumulated in the human body once they enter the food chain.

Some of heavy metals (such as selenium, cobalt, copper, iron, manganese, molybdenum, vanadium, strontium, and zinc) are micronutrients, which is essential for living organisms at trace quantities for maintaining their metabolism. However, pose a health risk to humans and the environment at high concentrations and lead to poisoning [19]. Furthermore, some of heavy metals like arsenic, chromium, lead etc., even at very low concentrations can be caused serious health problems to the human body like cancer or another poisonous effect [4, 20].

1.3.1 Nickel Occurrence

Among the possible contaminants, Ni^{+2} is one of the most common environmental pollutants. Ni is the 24th most abundant element in the earth's crust [20], and it is the fifth most abundant element by weight following iron, oxygen, magnesium, and silicon. It comprises around 3% of the earth's composition [21]. Nickel is a transition metal ion that has four oxidation states (+1, +2, +3, and +4), it is widely used in industry such as mining, smelting, textiles, fertilizer, electroplating, battery manufacturing, and pigment production [22, 23]. The Ni^{+2} in wastewater vary from a low value of 0.5 ppm to a high value of 1000 ppm. The maximum permissible safe limit of Ni^{+2} with industrial effluents into land water is 3 ppm [24]. Dermatitis (Ni itch) is the most frequent effect of exposure to Ni, such as coins and jewelry. [3]. Higher concentrations Ni^{+2} levels may cause cancer of the lungs, nose, and bone [25]. Acute effects of nickel toxicity include gastrointestinal symptoms like nausea, vomiting, abdominal discomfort and diarrhea, and neurological symptoms such as headache, giddiness, coughing, and shortness of breath. Nickel salts have an influence on

the pulmonary and digestive tract of the human. Exposure to soluble nickel compounds also causes cancer of the respiratory tract if the dose is greater than 1 µg Ni/L [3].

1.3 Techniques of Heavy Metal Removal

Several methods are using for heavy metal removal from effluents Including ion exchange, chemical precipitation, micro-membrane filtration, nano-membrane filtration and adsorption (figure. 3).

1.3.1 Ion Exchange

Ion exchange is the technique in which heavy metal ions are removed from the aqueous phase by exchanging charged ions, whether they are anions or cations between the exchange medium and the wastewater [26]. The resins used for the manufacture of ion exchange media are synthetic organic resins (i.e. zeolites, aluminosilicate) or natural resins (i.e. starch, cellulose, chitin) , or inorganic polymeric resins (i.e. silica gel, activated aluminas).

The removal of heavy metal ions by ion-exchange resins is influenced by several parameters like temperature, initial concentration of metal, pH, and contact time [3].

1.3.2 Chemical Precipitation

Coagulation and flocculation accompanied by sedimentation and filtration are used to remove heavy metals from wastewater. Destabilizing the colloids by neutralizing the forces that hold them apart called coagulation [27]. Most coagulants are widely used in wastewater treatment traditional processes, including coagulants such as aluminum salt, ferrous sulfate *(FeSO₄)*, and ferric chloride *(FeCl₃)*, resulting in the effective removal of wastewater particles and impurities by the neutralization of particulate matter and by impurities on the produced precipitates amorphous metal hydroxide [3].

1.3.3 Membrane Filtration

Recently, membrane filtration was used to treat effluent, because it has the ability to remove suspended solids and organic materials, in addition to inorganic pollutants such as heavy metals. Depending on the particle size that can be retained, different types of membrane filtration can be used, such as microfiltration, ultrafiltration, nanofiltration and reverse osmosis [17]. Ultrafiltration is a permeable membrane used to isolate heavy metals, macromolecules and suspended solids from an inorganic solution based on pore size (5–20 nm),(10–100 nm). While nanofiltration has a pore size range of 1.0 – 10.0 nm, and reverse osmosis has a pore size range of 0.1 – 1.0 nm, therefore, nanofiltration is known to be an intermediate process between ultrafiltration and reverse osmosis, nanofiltration is a promising technology to resist heavy metal ions [28]. The method of reverse osmosis uses a semi-permeable membrane, which allows the fluid that is purified to move through the membrane by applying pressure while removing the contaminants. Reverse osmosis is one of the methods used to remove a wide range of dissolved contaminants from water [3].
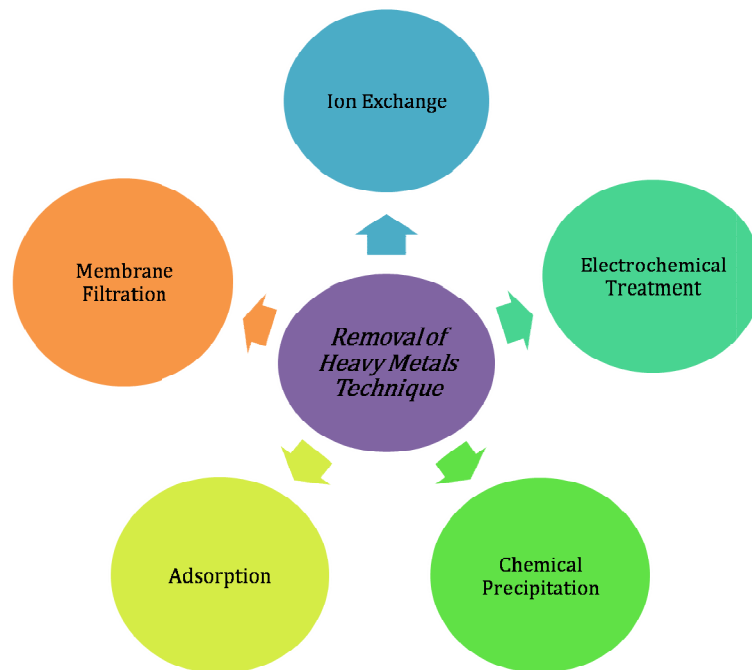
Figure 2. *Some of the common technique to remove heavy metals.*

1.3.4 Electrochemical Treatment

Electrochemical methods involve the plating of metal ions on the surface of the cathode and may recover metals in the elemental metal state. Various types of electrochemical treatment methods are available,such as electrocoagulation, electroflotation, electrochemical precipitation, and so on [3].

Electrocoagulation is a technique that uses currents to sacrifice an aluminum or iron anode so that the flocculation of an aluminum or iron hydroxide will absorb and precipitate metal ions [29]. When oxygen gas and fine H_2 bubbles produced by water electrolysis are formed at the cathode to float to the surface of the water, the solid/liquid process is called electroflotation [17].

Electrochemical precipitation has been used to optimize the removal of heavy metal from polluted wastewater; electrical capacity has been used to modify traditional chemical precipitation [3].

1.3.5 Adsorption Process

Adsorption is one of the main wastewater treatment techniques, due to its simple operation, low cost and the availability of a wide range of adsorbents. The method of adsorption as compared to other water treatment methods and the order of cost-effectiveness is adsorption > evaporation > aerobic treatment > anaerobic treatment > ion-exchange > electrodialysis > membrane filtration > reverse osmosis > precipitation > distillation > oxidation > solvent extraction [30]. Furthermore, adsorption is using to retain organic material, inorganic materials, biological pollutants and radioactive substances from polluted water, soil and air. Despite certain drawbacks, adsorption considers to be superior water treatment technique. A great deal of attention has been paid to nano-adsorbents due

9

to their high adsorption affinity in the removal of toxic and harmful substances from water and wastewater [4].

Most of these methods of treatment cannot be considered sustainable treatment technologies. Table 1 illustrates the advantages and disadvantages of a range of wastewater treatment methods and systems for heavy metals [31, 32].

Table 1.Advantages and disadvantages of the techniques to remove heavy metals.

Technique	Advantages	Disadvantages
Ion Exchange	Simple operation Large capacity High efficiency	Weak selectivity Waste products Regeneration High cost
Chemical precipitation	Simple operation Low cost	Ineffective for trace ions Waste products
Membrane Filtration	High efficiency High selectivity	Regeneration High cost High operation cost
Electrochemical Treatment	High efficiency High selectivity	High cost High operation cost
Adsorption	Wide pH range Low cost Simple operation Large capacity	Weak selectivity Waste products

1.5 Nanoscience in Water Treatment

Nanomaterials are the driving force behind the nanotechnology revolution and the main bottleneck for nanotechnology applications to address this global water crisis [33]. Nanoscience and nanotechnology propose that many of the current issues related to water quality can be solved or greatly improved by using nanoscale adsorbents, which called nano adsorbents. Therefore, effort has been done to find a novel nanomaterial with high affinity to treat and enhance water quality such as graphene, carbon nanotubes, and fullerenes [34].

1.5.1 Carbon Nanomaterial

Carbon, the sixth element of the periodic table, is denoted by the letter "C". Element carbon is revealed almost everywhere and it's one of the most ubiquitous in earth [31].

Carbon exist in several allotropes based on a hexagonal lattice, as illustrated in scheme1 Graphite is one of two naturally occurring types of crystalline carbon. The other natural allotrope is diamonds. The structure of the diamond is converted into graphite above 900°C. Graphite formed graphene layers of carbon atoms arranged in a honeycomb lattice with an interlayer spacing of 3.34 Å between sheets [22].

Carbon nanomaterials, with unique properties which include small size, high specific surface-area-to-volume ratio, large pore sizes, high reactivity, and a large number of active sites, have remained at the frontline of nanotechnology [31].Nanomaterials also provide unparalleled opportunities for developing more effective water purification catalysts [33]. This scheme highlights different types of carbon-based nanomaterials currently used in water treatment applications.
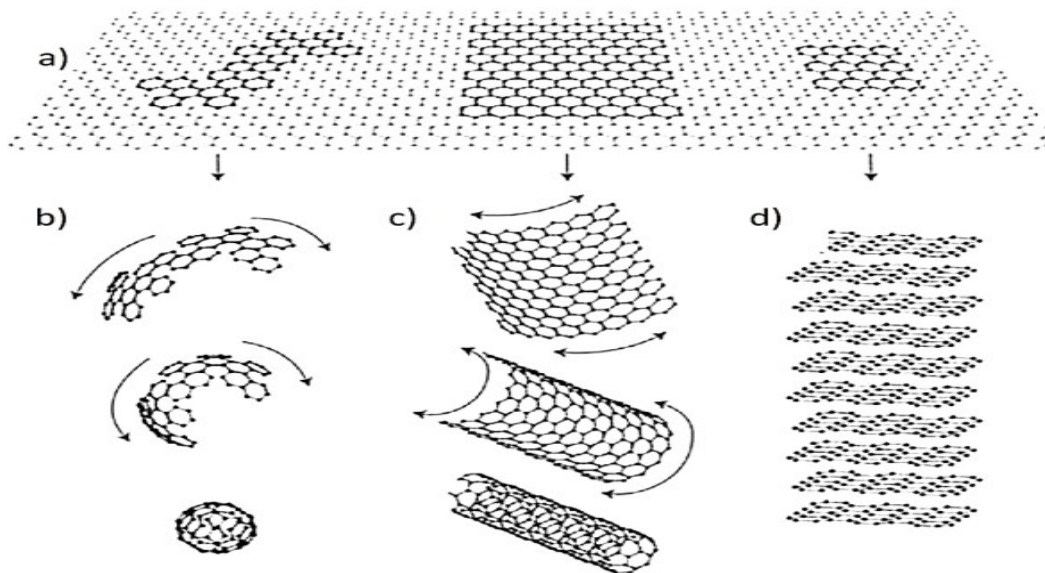
Scheme 1. *Schematic description of the various carbon nonmaterials, a) 2-D Graphene, b) 0-D Buckyballs, c) 1-D Nanotubes, d) 3-D Graphite.*[4]

1.5.1.1 Graphene

Graphene is known to be the parent element of some carbon allotropes, which is a fundamental structure block for graphite materials of all other dimensions, and can be converted into carbon nanotubes (CNT), 3D graphite or fullerenes by rolling, or stacking, wrapping, respectively [24].

Graphene has a special two-dimensional (2D) atom-thick structure of sp^2-hybridized carbon atoms densely packed in a honeycomb hexagonal pattern [35]. The special properties of graphene, such as high mobility, high thermal conductivity, and admirable electronic and mechanical properties, good chemical stability [26], high specific surface area (theoretically ~2630 m^2/g) [36], that makes graphene a powerful adsorbent material to

treat polluted water. The chemical modification of graphene makes it insoluble in water and confers sufficient surface properties to increase its adsorption ability [37].

In addition, graphene is excellent support for the anchoring of chemical functions or nanomaterials, and therefore graphene-based nanocomposites have been an active research area for novel materials. Graphene oxide (GO) is one of the most used graphene-based nanomaterials due to its low production cost [36].

1.5.1.2 Carbon Nanotube (CNT)

The discovery of carbon nanotubes (CNTs) has revolutionized the field of nanotechnologies [3]. Carbon nanotubes are part of a new class of carbon-based nanomaterials that has attracted the attention of the scientific community due to its many potential applications. CNTs consist of monomolecular carbon fibers with diameters varying from tens of nanometers to 200 nm, and up to a few micrometers in length [27]. Carbon nanotubes are classified as single-walled carbon nanotubes (SWCNTs) and multiple-walled carbon nanotubes (MWCNTs).

SWCNTs is a graphene sheet wrapped in the form of a cylinder with a single atom thickness and the wall of this cylinder is a hexagonal lattice of carbon atoms [38]. The MWCNTs are larger and consist of several single-walled tubes stacked inside each other. The term MWCNTs is limited to nanostructures with an outer diameter of less than 15 nm, above which such structures are called carbon nanofibers [39]. Nanotubes generally have a large length-to-diameter ratio. Thus, it considered as nearly one-dimensional structures [38, 39].

CNT's has unique chemical and physical properties lead to some extraordinary material properties, involving thermal conductivity that equivalent to diamonds, moreover, it has tensile strengths 100 times larger than steel [7]. In addition to mechanical strength, CNTs

contain novel electrical properties such as the high electrical conductivity as high as copper [39]. A combination of highly desirable properties indicates that CNTs are attractive components for a wide-range of applications in the real world [27]. For instance, CNTs are used in polymer formulations to provide electrical conductivity, mechanical strength, and in electronic components [40]. In other applications, CNTs are being considered for incorporation in bullet-proof vests, for use in a variety of precision electronic devices, as compounds to deliver targeted drugs, and as gene therapy imaging agents [27]. Carbon nanotubes are also widely used as materials to remove a variety of organic and inorganic pollutants from wastewater and water [17].

1.5.1.3 Fullerenes

In 1985 Buckminsterfullerene was discovered by Eric Rohlfing, Donald Cox and Andrew Kaldor, *(Kroto, Smalley and Curl, Nobel Prize in Chemistry 1996)*. The discovery of fullerene attracted a great deal of interest from researchers around the world [7]. It consists of an ellipsoid, cylindrical or spherical arrangement of dozens of carbon atoms [38]. The Buckminsterfullerene is a closed spherical structure with hexagonal and pentagonal rings made of carbon labeled C_{60}, and each carbon atom is sp^2 hybridized. It is named reference to Richard Buckminster Fuller, an American engineer who designed geodesic domes in the 1960s, and they are also called "buckyballs". Other possible fullerene structures are C_{20}, C_{24}, C_{28}, C_{32}, C_{36}, and C_{60}. C_{20} fullerene is the smallest fullerene possible [7]. As shown in figure2.

C_{20} C_{24} C_{28} C_{32} C_{36} C_{50} C_{60}
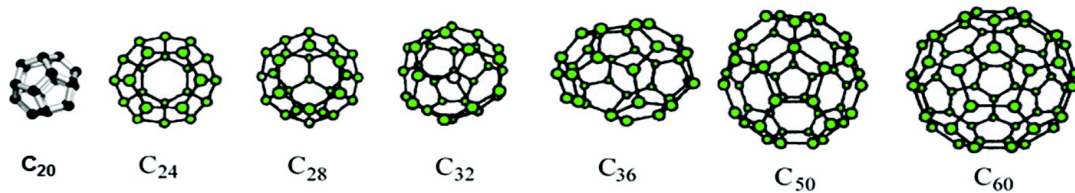
Figure 3. *Types of Fullerenes.*[41]

Physical and chemical properties of carbon fullerenes different from both diamond and graphite, C_{60} is a fullerene favorite in research and development as it is widely available in high purity and relatively large quantities. Molecularly, the C_{60} contains 60 carbon atoms arranged on a spherical anthropomorphic form, similar to the shape of a soccer ball [27, 42]. Expected applications for the C_{60} are increasing, including fullerene, and currently include fuel cell production, drug delivery agents, superconductivity devices, and diamond manufacturing [27]. One of the most important potential applications for C_{60} functional molecules is photophysical and medical applications. The most important potential medical applications of C_{60} derivatives are focused on their demonstrated antiviral activity and their use as photosensor in photodynamic therapy [42].

2. Research Objectives

The main aims of this study are:

I. Synthesis and characterizations of graphene oxide (GO-450 nm), and reduced the size of graphene oxide (GO-200 nm).

II. A study of removal nickel ions by graphene oxide using adsorption process.

III. Study the variable parameters that affect the adsorption process such as (adsorbent dose, contact time, pH, temperature..etc)

Chapter Two:

Literature Review

2.1 Adsorption

Adsorption is a surface phenomenon described as a process of mass transfer involving the accumulation of substances at the interface of two phases, such as liquid-liquid, gas-liquid, gas-solid or liquid-solid interfaces [43]. As shown in figure 4 the substance which adsorbs another substance is called an adsorbent. And the substances that retained onto adsorbent is called adsorbate [32].
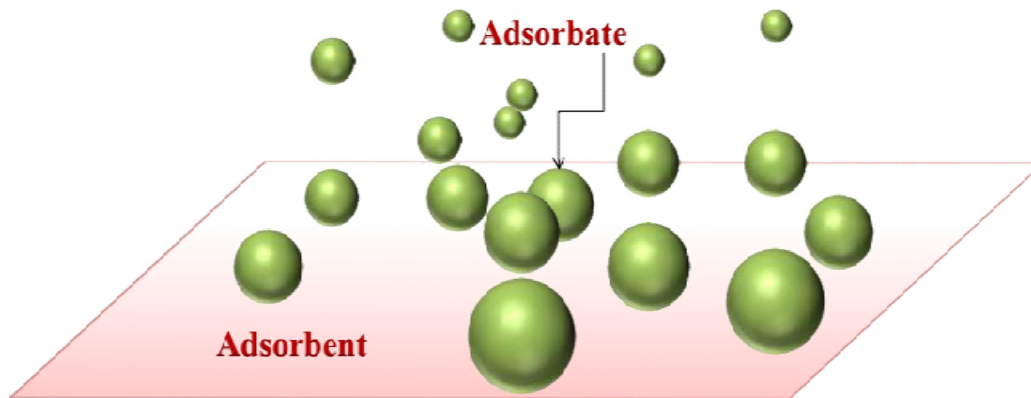
Figure 4. *Adsorption process between adsorbent and adsorbate.*

There are two main types of adsorption: chemical adsorption and physical adsorption.

I.   Chemical adsorption

Chemical adsorption also referred to as chemisorption; the attraction forces between the adsorbate and the adsorbent is very strong, since these forces are chemical bonding like covalent or ionic bonds. Chemisorption are typically an irreversible process [44].

II.   Physical adsorption

Physical adsorption or physisorption; it includes a weak force result from the weak forces electrostatic interactions, between adsorbate and adsorbent, these forces are usually intermolecular forces such as Van der Walls forces. Therefore physical adsorption is often referred to as van der Walls adsorption [26]. The adsorbed material in this type of

adsorption is not attached to a specific site on the solid surface and can move over the surface. Hence, understanding the surface properties of adsorbents including surface area and polarity is essential. Physical adsorption is reversible type [44].

2.1.1 Adsorption Material

Several solid materials have been used as adsorbents to remove Nickel (II) and other metals [37]. This material can take on a wide variety of chemical forms and various geometric surface structures. Adsorbents typically can be classified into five categories: (1) natural materials such as sawdust, wood, fuller's earth or bauxite; (2) natural materials treated to develop their structures and properties such as activated carbons, activated alumina or silica gel; (3) manufactured materials such as polymeric resins, zeolites or aluminosilicates; (4) agricultural solid wastes and industrial by-products such as date pits, fly ash or red mud; and (5) Bio- sorbents such as chitosan, fungi or bacterial biomass [45].

Crini 2005 introduced a simple classified for adsorbents materials simplified consisting of conventional and nonconventional materials as shown in figure 5 [45]. The conventional adsorbent list includes commercial ion-exchange resins, commercial activated carbons (CAC), and inorganic materials like commercial activated aluminas (CAA), silica gel, and zeolites. The list of non-conventional adsorbents includes industrial by-products, natural materials such as clays, industrial by-products such as red mud, biosorbents such as chitosan and diverse adsorbents such as alginates [44, 45]. In addition, researches has also been conducted on nanomaterials such as carbon nanotubes, and graphene due to their high adsorption capacity [44].

The graphene family, such as graphene, graphene oxide (GO), and reduced graphene oxide (rGO) have been comprehensively studied since their discovery due to their unique physical and chemical properties [34].

GO is a two-dimensional layer of sp^2 hybridized carbon atoms decorated with abundant oxygen groups like carboxyl, hydroxyl, epoxy, etc., and these groups have the ability to bind with organic and inorganic substances with both chemical and/or physical interactions. Moreover due to its highly hydrophilic surfaces, open up flake morphology and high adsorption capacity towards different chemical substances, several reports have been focused on GO as a promising nanosystems in wastewater treatment. Moreover, it exhibits no obvious toxicity under low dose (0.2 mg) and middle dose (0.2 – 0.25 mg) [46–48].
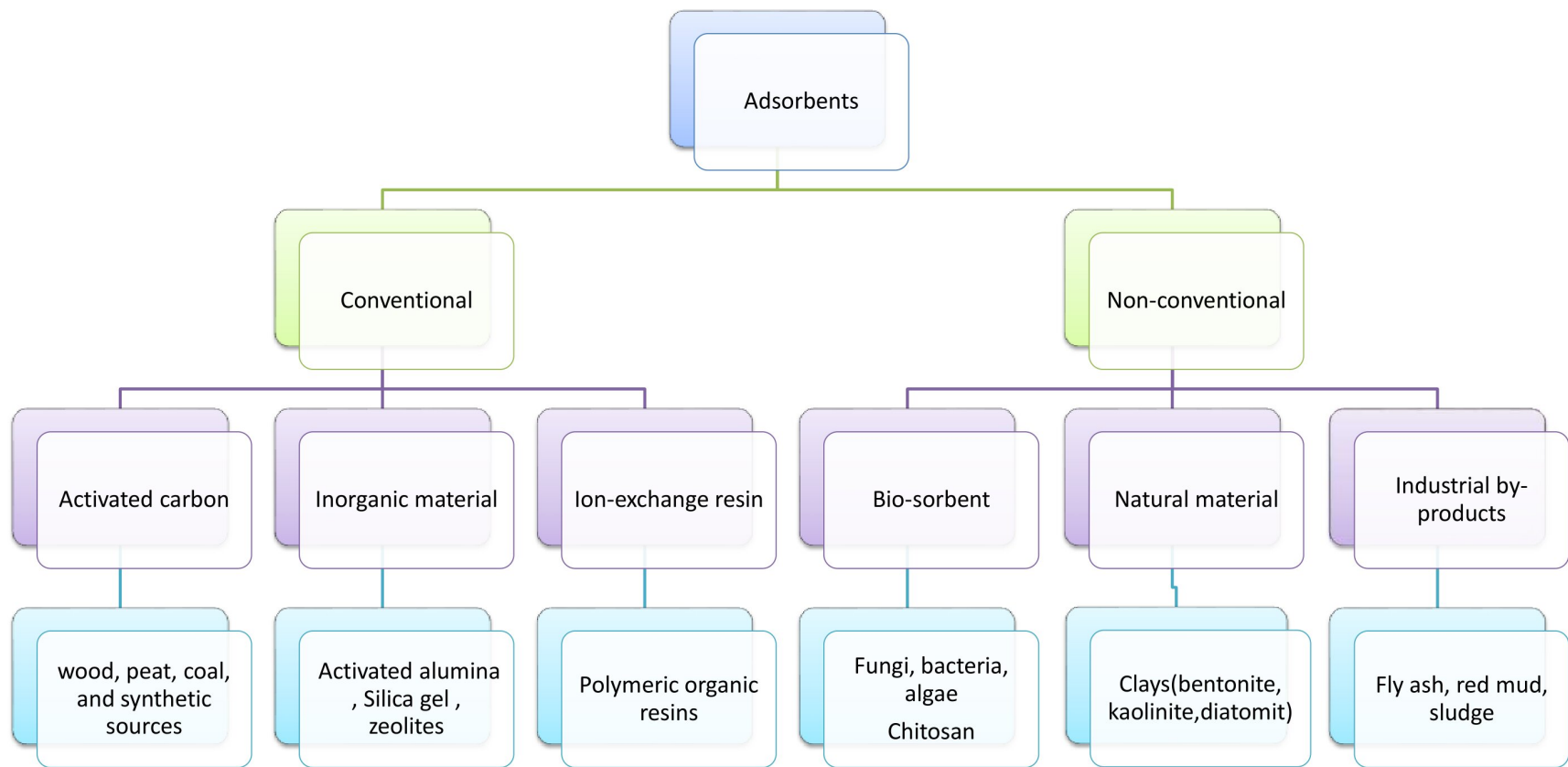
Figure 5.*Conventional and nonconventional materials used in water treatment.*

2.1.2 Mechanism of Adsorption

The common cationic pollutants in wastewater are Pb(II), Hg(II), Cd (II), Cu(II), Ni(II), Co(II), and Zn(II). In general, the adsorption of metal ions is based on the three mechanisms of adsorption: electrostatic interaction, ion exchange, and complex formation [49].

A driving force for adsorption is the electrostatic attraction between the positively charged heavy metal ions and the negatively charged GO sheets as shown in figure 6. The electrostatic interaction contributed to the adsorption of heavy metal ions on GO but was not the dominant factor [50].
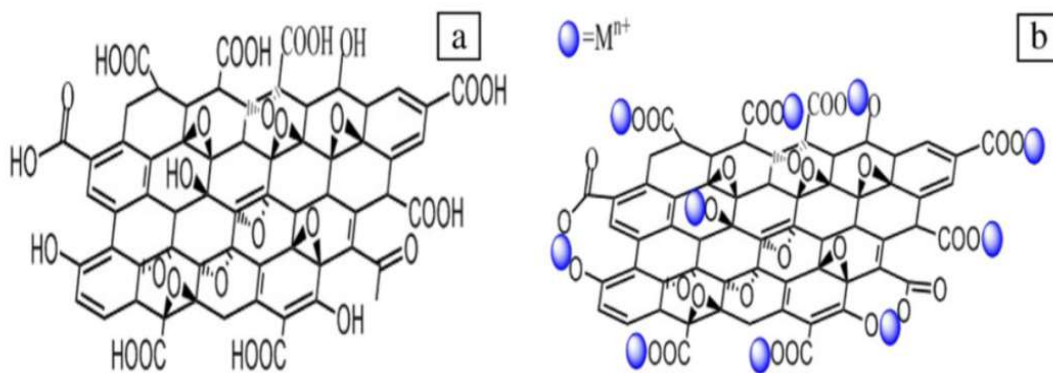
Figure 6. *(a) Structure of GO (b) interaction of GO with heavy metal cations.*[50]

One mechanism for the adsorption is the ion exchange reaction between the heavy metal ions and the proton on –COOH or –OH oxygen functional groups. In the adsorption process, the proton on –COOH or –OH was released to the solution, resulting in a lower equilibrium solution pH than the initial value [50]. Exchange of M^{+2} and H^+ on –COOH or –OH oxygen groups responsible for M^{+2} adsorption onto GO, is represented by the following equations [51]:

$$-COOH + M^{+2} \rightarrow -COOM^+ + H^+ \tag{1}$$

$$-OH + M^{+2} \rightarrow -OM^+ + H^+ \tag{2}$$

$$-2COOH + M^{+2} \rightarrow -COOMOOC- + 2H^+ \tag{3}$$

$$-2OH + M^{+2} \rightarrow -OMO- + 2H^+ \tag{4}$$

$$-COOH + M^{+2} + -OH \rightarrow -COOMO- + 2H^+ \tag{5}$$
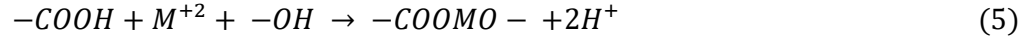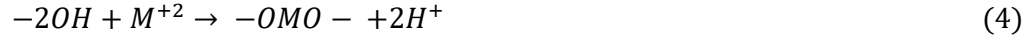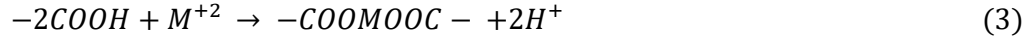
2.2 Adsorption Equilibrium

Isotherms of adsorption are used to quantify the amount of adsorbate that can be adsorbed onto adsorbent at constant temperature and equilibrium conditions. The equilibrium solid-phase adsorbate concentration can be calculated from an experiment that varies the adsorbent dose and the initial adsorbate concentration, and a relationship may be established with the equilibrium liquid-phase concentration. This adsorption equilibrium relationship is called the isotherm and enables to calculate the adsorption capacity of the adsorbent at any given liquid-phase adsorbate concentration [44].

The percentage removal ($\% R$) and adsorption capacity of equilibrium, q_e (mg/g) of the aqueous heavy metal ions is determining by using the equation of mass balance (1-2):

$$(\% R) = \frac{C_i - C_e}{C_i} \times 100 \tag{1}$$

$$q_e = \frac{(C_i - C_e)}{m} \times V_L \tag{2}$$

Where C_i and C_e are the initial and equilibrium concentrations of metal ions in mg/l, respectively; V_L is the sample volume in liter, and m is the mass of adsorbent in gram (g) [52].

2.2.1 Adsorption Isotherm Models

Equilibrium modeling of adsorbent-adsorbate interactions was used to determine the conduct of experimental data in order to optimize the operating parameters of the water treatment reaction. Numerous models were used to measure the efficiency of adsorption by given adsorbents. Langmuir and Freundlich models are the most commonly used isotherm models in the literature. These models illustrated below:

2.2.1.1 Langmuir Isotherm

In 1916 Irving Langmuir developed an adsorption isotherm model that is used to describe the equilibrium between adsorbate and adsorbent system at a fixed temperature. It is based on a number of assumptions and applied to estimate the adsorption capacity of the adsorbent used [17]. These assumptions are:

  i.   Adsorption is assumed to be monolayer.

  ii.   The surface of the adsorbent is homogeneous.

  iii.   Adsorbed molecules do not interact, and all adsorption occurs by the same mechanism.

  iv.   Only one monolayer is formed at maximum adsorption: adsorbate molecules do not deposit on other, adsorbate molecules that are already adsorbed, but only on the free surface of the adsorbent.

The nonlinear isothermal equation for the Langmuir is:

$$q_e = \frac{q_m \times K_l \times C_e}{1 + (K_l \times C_e)} \tag{3}$$

The linearized Langmuir isotherm is described as:

$$\frac{C_e}{q_e} = \frac{1}{K_l \times q_m} + \frac{C_e}{q_m} \tag{4}$$

Where, q_m is the maximum adsorption capacity ($mg\ adsorbate/g\ adsorbent$), q_e is the adsorption capacity at equilibrium (mg/g), and C_e is the concentration of metal ions at equilibrium (mg/L). A plot between the specific adsorption (C_e/q_e) as y-axis versus the equilibrium concentration (C_e) as x-axis will show whether or not the experimental data obeys this model [14]. A straight line from the (C_e/q_e) vs. (C_e) graph should indicate $1/q_m$ and $1/K_l \times q_m$ as the slope and intercept, respectively [52]. R_L is a unitless factor of separation used to describe whether or not the adsorption process is favorable. Table 2 explains the essential characteristics of the Langmuir isotherm. This factor is represented by the following equation:

$$R_L = \frac{1}{1 + K_l C_i} \tag{5}$$

Where, K_l is the Langmuir constant (L/mg) related to the energy of adsorption, C_i is the maximum initial concentration of adsorbate (mg/L).

Table 2. Essential characteristics isotherm of the Langmuir model [53].

Value of R_L	Adsorption
$R_L > 1$	Unfavorable
$R_L = 1$	linear
$0 < R_L < 1$	Favorable
$R_L = 0$	Irreversible

2.2.1.2 Freundlich Isotherm

Freundlich published the first mathematical fit to an isotherm in 1906. His equation is a purely empirical formula that has proved suitable for the description of short-term and monocomponent adsorption of metal ions by various materials [17]. Freundlich isotherm is an empirical expression that accounts for surface heterogeneity through multilayer adsorption; it's applicable to both (chemisorptions) and (physisorption) [4]. And the isotherm of Freundlich adsorption is described as [20]:

$$q_e = K_f C_e^{\frac{1}{n}} \tag{6}$$

The Freundlich equation linear form can be expressed as follows:

$$\ln q_e = \ln K_f + \frac{1}{n} \ln C_e \tag{7}$$

Where, q_e is the adsorption capacity at equilibrium (mg/g), C_e is the concentration of metal ions at equilibrium (mg/L), K_f is the constant associated with the adsorption capacity of the adsorbent, and n is the constant related to the adsorption intensity [54]. The constants (n) and (K_f) of Freundlich isotherm are calculated from the slope and intercept

of the linear plot ($ln\ q_e$) versus ($ln\ C_e$) [25]. Table 3 illustrated Freundlich coefficient, 1/n value to indicate the type of isotherm [43].

Table 3. The characteristic constant of 1/n value of Freundlich isotherm.

$\dfrac{1}{n}$ value	Type of isotherm
$\dfrac{1}{n} = 0$	Irreversible
$0 < \dfrac{1}{n} < 1$	Favorable
$\dfrac{1}{n} > 1$	Unfavorable

2.2.2 Kinetic Isotherm Models

Adsorption kinetics. Understanding the adsorption kinetics is very important in order to understand the extent to which the adsorbent can uptake the adsorbate. It also provides an overview of the time and path of reaction through which to approach equilibrium through the process. This is a function of the adsorbent properties and the process's operating parameters [55].

The pseudo-first-order kinetics and the pseudo-second-order kinetic model are the most commonly used kinetic expressions to explain the solid/liquid adsorption processes.

2.2.2.1 Lagergren's Pseudo-First-Order

The pseudo-first-order model relates the process rate to the quantity of solute removed per unit mass of media, and given by the following equation [56]:

$$\frac{dq_t}{dt} = K_1(q_e - q_t) \tag{8}$$

Linearized plotting of data as indicated by equation 9:

$$ln\ q_e - q_t = ln\ q_e - K_1 t \tag{9}$$

Where: q_t Is the adsorption capacity at any time t (mg/g), q_e is the adsorption capacity at equilibrium (mg/g), k_1 is the first-order rate constant adsorption $(1/min)$ and (t) time(min). Values of (k_1) and q_e for different initial concentrations of ions were calculated from the slope and intercept respectively of the linear plot of (t) as x-axis versus $(ln\ q_e - q_t)$ as the y-axis [14].

In several cases, the Lagergren's equation does not fit well with the entire contact time range and is generally applied during the initial phase of the sorption processes. In addition, while the pseudo-first-order "Lagergren" kinetics provide an excellent fit with the experimental kinetic data in some cases, it failed to predict the q_e theoretically deviating from the theory [17].

2.2.2.2 Ho's Pseudo-Second- Order

The kinetic equation for pseudo-second-order adsorption is expressed as;

$$\frac{dq_t}{dt} = K_2 (q_e - q_t)^2 \tag{10}$$

The rearrangement of equation 10 gives the following:

$$\frac{t}{q_t} = \frac{t}{q_e} + \frac{1}{k_2 q_e^2} \tag{11}$$

Where: q_e is the adsorption capacity at equilibrium (mg/g), q_t is the adsorption capacity at any time t (mg/g), (t) time(min), k_2 is the rate constant for the pseudo-second order adsorption $(g/mg.min)$ [57].

The plot of (t) at the x-axis and t/q_t at the y-axis of the equation gives a linear relationship from which (k_2) and (q_e) can be determined from the intercept and slope of the plot, respectively [25].

2.2.3 Adsorption Thermodynamics

To conclude whether the process is spontaneous or not, the thermodynamic considerations of an adsorption process are necessary [58]. Thermodynamic parameters such as enthalpy $\Delta H°$ and entropy $\Delta S°$ are calculated using Van't Hoff equation:

$$ln\ K_D = -\frac{\Delta H^°}{RT} + \frac{\Delta S^°}{R} \tag{12}$$

Where: $\Delta H°$ is the enthalpy change(kJ/mol), $\Delta S°$ is standard entropy$(J/mol.K)$, K_D is the distribution coefficient in(ml/gm), R is the ideal gas constant$(8.314\ J.mol/K)$, and T the absolute temperature in$°K$. The values of $\Delta H°$ and $\Delta S°$ can be calculated from the slope and intercept of plotting $ln\ K_D$ versus$(1/T)$ respectively [59].

The values for standard free energy are determined from the equation:

$$\Delta G^° = \Delta H^° - T\Delta S^° \tag{13}$$

Where:$\Delta G°$ is the standard Gibbs free energy (kJ/mol), and the characteristics data of $\Delta G°$, $\Delta H°$ and $\Delta S°$ are together summarized in table 4 [60].

Table 4. The characteristics values of Van't Hoff equation.

Value of Van't Hoff equation	Negative (−)	Positive (+)
ΔH°	Exothermic	Endothermic
ΔS°	Decreased randomness	Increased randomness
ΔG°	Spontaneous	Non-Spontaneous

2.2.4 Factors Affecting Adsorption Capacity

There are an increasing number of different types and quantities of nano adsorbents used in the removal of heavy metals from water, and the adsorption capacity of the diverse adsorbents for each heavy metal ions is also different. [51]. Here we will introduce some of the factors affecting the adsorption properties of nanomaterials.

I.   The chemical and physical properties of adsorbents.

Adsorption is a type of surface phenomenon [4, 18]. The larger the adsorbent's specific surface area, the greater the adsorption capacity. The specific surface area, particle size, pore structure, and distribution are different when the types and preparation methods of adsorbents are different, resulting in the effect of adsorption also being different. In addition, the surface chemical structure and surface charge properties of adsorbents also have great influence on the adsorption process [51].

II.   *The concentration and properties of the adsorbate.*

The initial concentration of heavy metals affects the sorption capacity because it acts as a driving force to overcome metal resistance or the transfer of mass from liquid to the solid phase [61]. In general, some researchers claim that the higher the initial concentration of heavy metals, the more the adsorption of the metal by the adsorbent [32].

III.   *Contact Time*

The contact time affects the adsorption capacity, where the time required for the adsorption process differs depending on the adsorbent nature and the adsorption sites available [32,60]. The adsorption rate depends on the time required to reach equilibrium of the adsorption. The faster the speed of adsorption, the shorter the time it takes for balance to be achieved [51].

IV.   *The pH of the solution*

pH is one of the most important adsorption process variables that can directly affect the adsorption of metal ions by adsorbents [62]. Since the adsorption occurs in most cases through the association of hydronium or hydroxide ions, the process is greatly affected by the medium's pH [51].

V.   *Temperature*

Rising temperature may result in an increase either in the number of adsorption sites available on the GO surface or in the diffusion rate of heavy metal ions, thereby accelerating the adsorption rate. The adsorption capacity on GO for heavy metal ions increases with increasing the temperature [63].

2.2 Adsorption Studies on Different Adsorbents

The main challenge in the context of adsorption is to select the most promising types of adsorbents, mainly in terms of low-cost, high capacity (often expressed by the q_{max} value), high adsorption rate, high selectivity, and rapid kinetics [45]. Results of previous studies on the adsorption of nickel ions by different adsorbents are summarized table 5.

Table 5: Comparison of the maximum adsorption capacity q_m (mg/g) of Ni^{+2} using various adsorbent.

Adsorbent	$q_m(mg/g)$	Ref.
Fly ash	0.03	[64]
Oxidized CNTs	1.83	[65]
Oxidized MWCNTs	3.73	[66]
Activated carbon prepared from almond husk	30.77-37.18	[67]
Graphene nanosheet/δ-MnO$_2$ composite	46.55	[68]
Coir pith	9.50	[69]
Carbon aerogel	12.87	[70]
Scrap tire	25.00	[71]
Υ - Fe$_2$O$_3$	23.60	[72]
BT leaf powder	1.527	[73]
Natural zeolite	8.69	[74]
Modified zeolite (NaCl)	10.46	[74]
Bentonite	90	[22]

2.4 Adsorption Studies to Removal Heavy Metals by GO.

Several materials have been used as adsorbents to remove heavy metal ions. Recently, the use of nanomaterials as efficient and viable alternatives to activated carbon has grown in interest due to their unique physical and chemical properties [75].

Nanoadsorbents like GO not only have a larger surface area, but also have some distinctive features such as catalytic potential and high reactivity [18, 75]. The literature relating to these studies is documented in table 6 below:

Table 6: Comparison of the maximum adsorption capacity q_m (mg/g) of several heavy metal ions on GO.

Adsorbent	Metal ions	$q_m(mg/g)$	Conditions	Ref.
GO	Ni^{+2}	35.6	T= 20 ^{0}C	[14]
GO	Ni^{+2}	38.61	pH=6, T=25 ^{0}C, t=50 min	[77]
GO	Ni^{+2}	20.19	T=25 ^{0}C,	[20]
GO	Cu^{+2}	277.77	pH=6,T= 25 ^{0}C, t=60 min	[78]
GO	Co^{+2}	21.28	pH=5.5,T= 25 ^{0}C, t=60 min	[35]
GO	Pd^{+2}	98.328	T= 25 ^{0}C	[79]
GO-SDS	Ni^{+2}	55.16	pH=6, T= 298 K	[80]
GO	Ni^{+2}	20.19	pH=6, T= 298 K	[80]

Chapter Three:

Methodology

3. 1 Materials and Methods

This chapter outlines the experimental procedures that were used during the investigation. The various chemicals used, methods used for GO synthesis, reduced GO size, and Ni (II) adsorption studies.

3.1.1 Chemicals

Graphite powder, <20μm, potassium permanganate (99%), and nickel sulfate hexahydrate (99%) were purchased from Sigma Aldrich. Sulfuric acid (95%), nitric acid (70%), hydrochloric acid (32%), sodium chloride (99.9%), hydrogen peroxide (30%), sodium hydroxide (99%) (Technical grade).

3.1.2 Instrumentation

Graphene oxide was characterized using Perkin-Elmer, Spectrum Two, FT-IR spectrometer that has a range of (4000–400 cm^{-1}). Ultrasonic processors Sonics, Materials VC-750-220, Fisher Scientific. The SEM images were obtained using scanning electron microscopes an FEI, NOVA NanoSEM-200 with an acceleration voltage of 15 kV the measurement were carried out at IFW Deresden, Germany. The Ni (II) concentrations were measured by an Aqualabo Company UV-Visible line 9100 spectrophotometer that has a photometric range of 320- 1100 nm. Other instruments are pH meter, water bath sonicator and suction filtration assembly.

3.2 Methods
3.2.1 Preparation of Graphene Oxide (GO).

As shown in figure 7,and scheme 2 graphite oxide was prepared by using the Hummers method and conventionally by the oxidation-exfoliation reaction [80, 81]. Briefly, 1.0 g of

graphite and 50 g NaCl were grounded in mortar for 20 min, the ground graphite was dissolved in distilled water, filtrated, washed several times and dried in an oven at 40°C for 6 h. The filtrated graphite was stirred in 23 ml 95% H_2SO_4 overnight. The mixture was placed in an ice bath (below 10 °C) for starting the oxidation step, 3.0 g $KMnO_4$ was added slowly over 3 hours with continuous stirring. Afterward, the mixture was heated up to 35 °C for 30 min and to 50 °C for 45 min, respectively. The mixture was cooled down then 46 ml of distilled water was added slowly to the solution, and the solution temperature was increased to 98-105 °C with stirring for 45 min. A 140 ml distilled water and 10 ml of 32% H_2O_2 were added gradually to terminate the reaction. The final product was filtered and washed 5 times with 5% HCl and distilled water. Lastly, the graphite oxide was dried in an oven at 50 °C for 6 h [83].

Synthesis of graphene oxide nanoparticles

The graphene oxide nanoparticles were prepared depends on the previous protocol (scheme 2) [84]. Shortly, 1.0 mg/ml of graphite oxide was sonicated in an ultra-sonication bath under controlled conditions (power and time) [35].
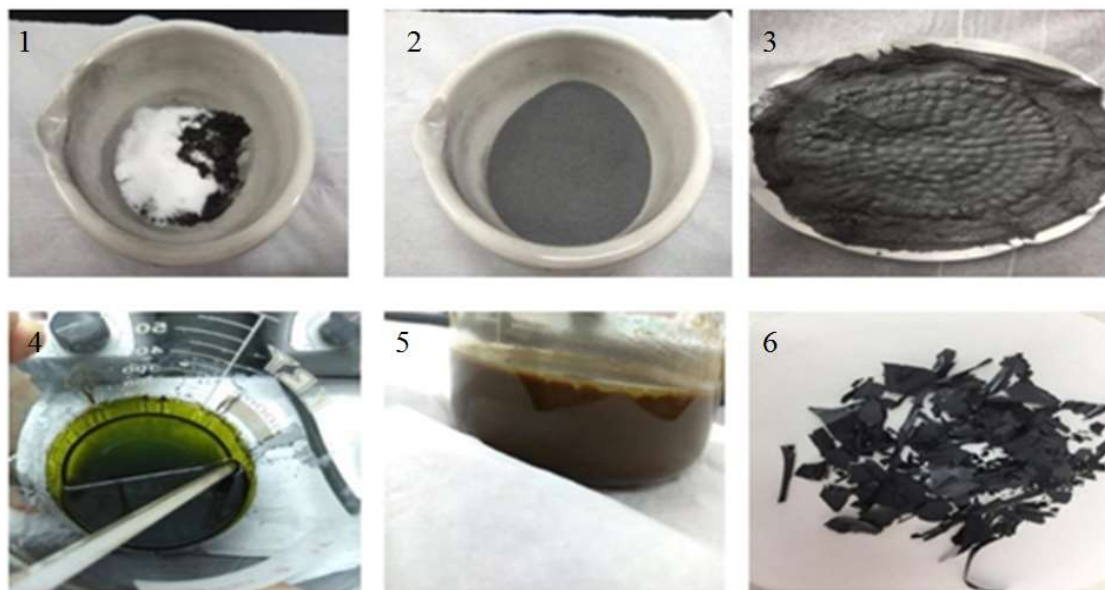
Figure 7.*Preparation steps of graphene oxide (GO)*
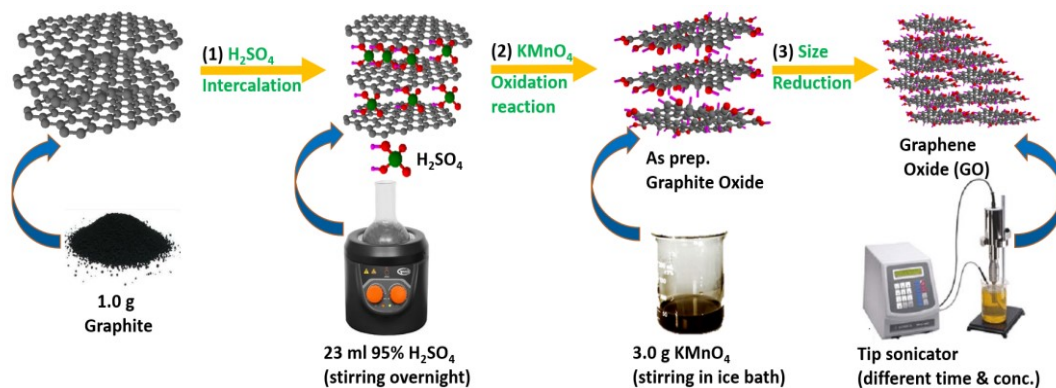
Scheme 2. *Schematic representation of graphene oxide formation by using tip sonicator.*

3.2.2 Preparation of Solution

A 1000 ppm stock solution of Nickel (II) sulfate hexahydrate was prepared by dissolving 0.4478 g in 100 ml distilled water. The stock solution was used for the preparation of diluted solutions (200, 300, 400, 500, 600, 700, 800, and 900 ppm). As shown in figure 8.

Figure 8. *Different concentrations of $NiSO_4.6H_2O$ (200 -900 ppm) from left to right.*

3.2.3 Adsorption Study

All experiments have been performed in a batch adsorption mode. By adding either 0.1 M HCl or 0.1 M NaOH solution, the pH of this solution was adjusted to the required values. 3.0 ml of the solution (NiSO$_4$.6H$_2$O) was transferred to the bottle. In order to produce the required adsorbent dosage a known mass of graphene oxide was added. The bottles and their contents were placed in the water bath sonicator at the required temperature for a specific time interval. The solution was filtered by suction filtration; and quantified using UV-Visible spectroscopy. For the removal of Ni (II) by graphene oxide (GO) and reduced size of graphene oxide, the effect of adsorbent dose, contact time, initial concentration of Ni (II), pH, and temperature were optimized. The procedure described for each studied parameter is given below.

I.   *Effect of pH*

To study the effect of pH on Ni^{+2} adsorption by GO, the adsorption test was carried out at broad pH ranges (2 – 10). The experiment was carried out as follows: then 3.0 ml solutions containing (400 ppm of Ni^{+2}) the pH of each solution was adjusted to the target pH either by,0.1 M HCl or 0.1 M NaOH solutions. The (GO) and reduced size of GO dose of 20 mg was introduced into each bottle and kept in contact at the contact time of 60 minutes at the constant temperature of 25.0 °C. Subsequently, these samples were agitated by water bath sonicator, after that the samples were filtered by suction filtration. Ni^{+2} concentrations of the ions were determined by UV-Visible spectroscopy by measuring the absorbance of each solution at 393 nm. A systematic methodology of this study is shown in Scheme 3.

```
┌─────────────────────────────────────────────────────────────┐
│   Put 3.0 ml of Ni⁺² solution 400 ppm in 10 bottles          │
└─────────────────────────────────────────────────────────────┘
                              ▼
┌─────────────────────────────────────────────────────────────┐
│                   Adjusted pH from 2 to 10                    │
└─────────────────────────────────────────────────────────────┘
                              ▼
┌─────────────────────────────────────────────────────────────┐
│     Add 20 mg of (GO-450 nm),(GO-200nm) into each bottles     │
└─────────────────────────────────────────────────────────────┘
                              ▼
┌─────────────────────────────────────────────────────────────┐
│               Agitated at 25 °c  for 60 min                   │
└─────────────────────────────────────────────────────────────┘
                              ▼
┌─────────────────────────────────────────────────────────────┐
│               Filtrate analyzed for  Ni ⁺²                    │
└─────────────────────────────────────────────────────────────┘
```
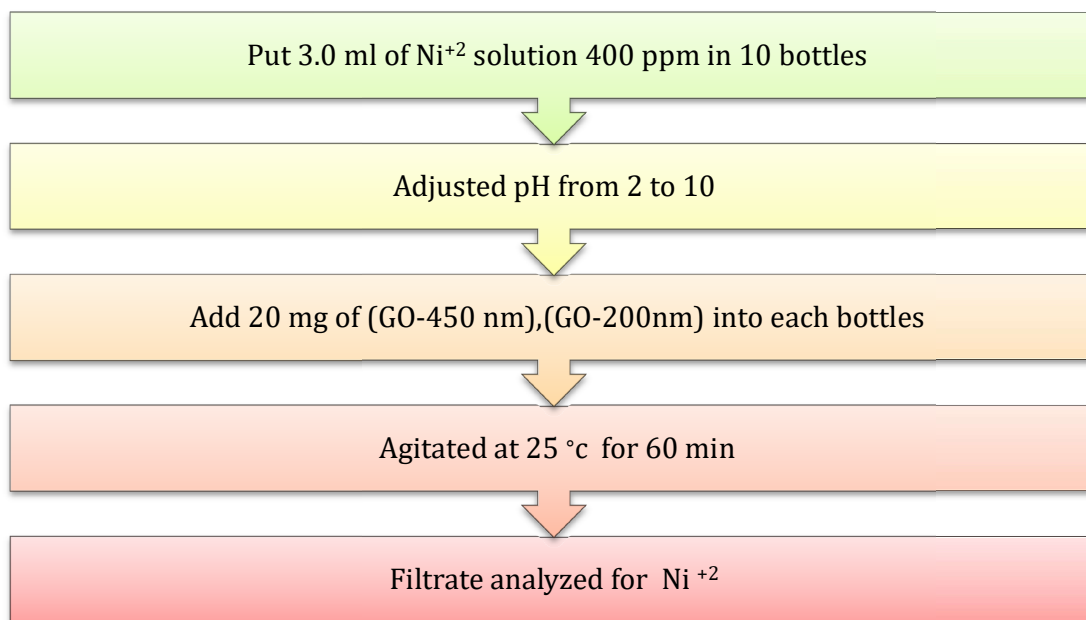
Scheme 3. *A systematic methodology of PH study*

II.   *Effect of adsorbent dose*

The solution was prepared with an initial Ni^{+2} ion concentration of 400 ppm, and then adjusted for each solution for pH adsorption previously determined in section I (effect of pH), in 18 bottles; 3.0 ml of this solution was poured to each bottle. Various doses of GO and reduced size of GO i.e. 1, 2.5, 5, 10, 20, 30, 40, 60, and 80 mg was added into each bottle. These samples were agitated at a water bath sonicator and the temperature was 25 °C. After that filtrate was separated by suction filtration. The concentration of ions Ni^{+2} was spectrophotometrically determined by measuring the absorbance of each solution at 393 nm. A systematic methodology of this study is shown in Scheme 4.

| Put 3.0 ml of Ni^{+2} solution 400 ppm in 18 bottles |
| Adjusted pH to optimum pH of adsorption |
| Add (GO-450 nm),(GO-200 nm) 1- 80 mg into each bottles |
| Agitated at 25 °c for 60 min |
| Filtrate and analyzed for Ni^{+2} |
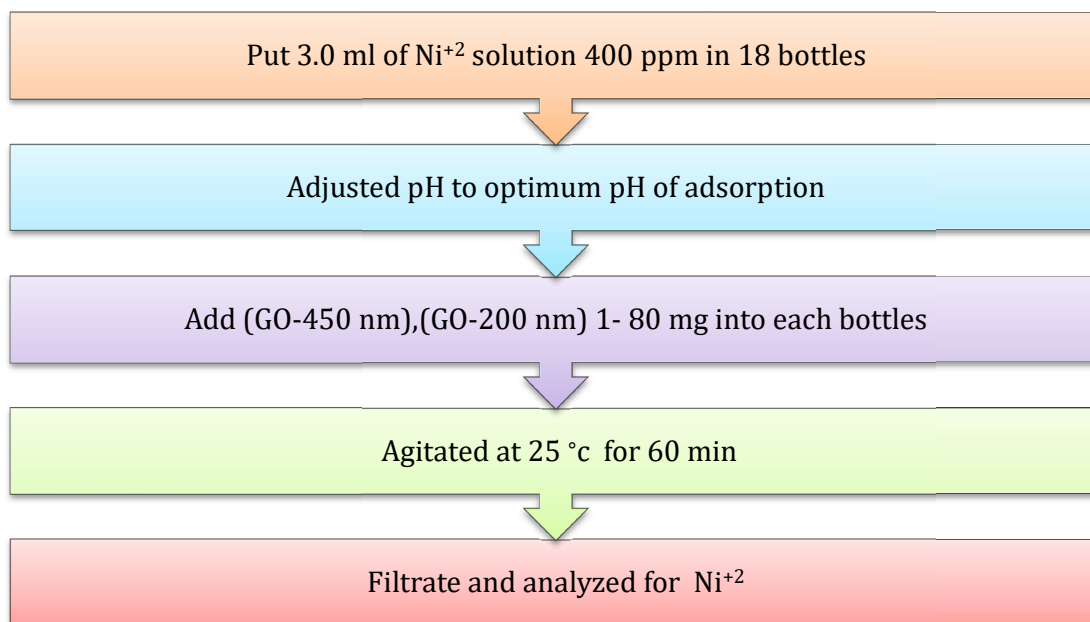
Scheme 4. *A systematic methodology of adsorbent dose effect*

III. *Effect of contact time*

Batch experiments were carried out to estimate the time needed to obtain equilibrium conditions for Ni^{+2} ion adsorption on GO, and reduced size of GO. The solution was prepared with an initial Ni^{+2} ion concentration 400 ppm, and then adjusted to the optimum pH adsorption previously determined in section 1. A 3.0 ml of this solution was poured into 10 bottles containing (20 mg of GO or reduced size of GO). Samples were agitated for 10, 30, 60, 90 min, and 120 min. then samples were filtered by filter paper through suction filtration, theNi^{2+}concentration in filtrate was determined spectrophotometrically by measuring the absorbance of each solution at 393 nm. A systematic methodology of this study is shown in Scheme 5.

Put 3.0 ml of Ni^{+2} solution (400 ppm) in 10 bottles
Adjusted pH to optimum pH of adsorption
Add (GO-450 nm),(GO-200 nm) 20 mg into each bottles
Filtered after 10, 30, 60, 90, 120 min
Filtrate analyzed for Ni^{+2}
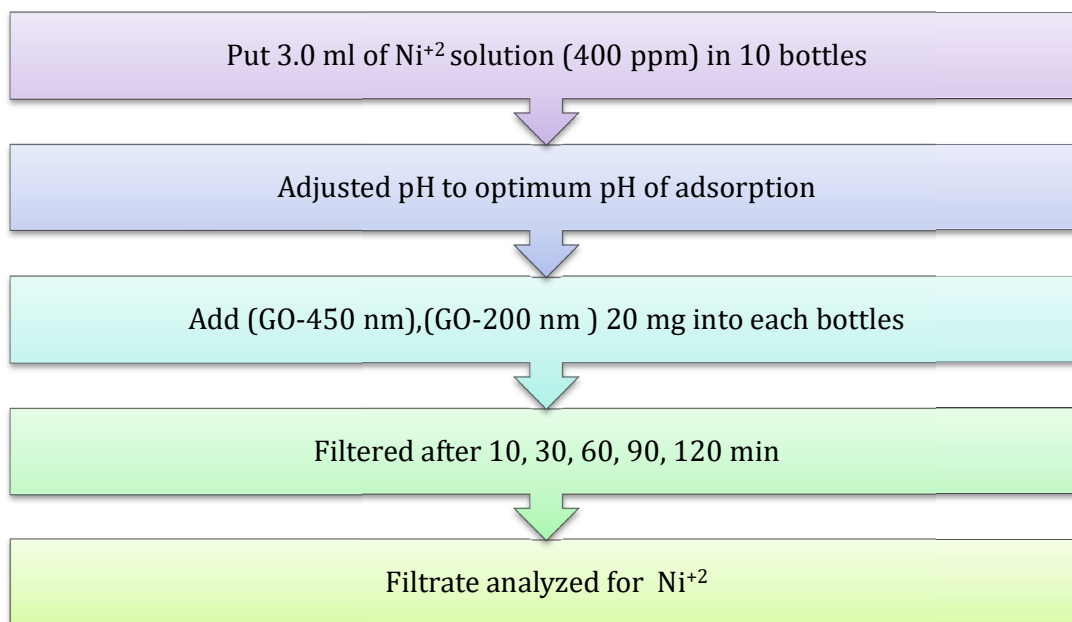
Scheme 5. *A systematic methodology of contact time effect.*

IV.   *Effect of temperature*

Adsorption experiments were performed to study the effect of temperature on the concentration of Ni^{+2} ions. A systematic methodology of this study is shown in Scheme 6. The solutions with an initial Ni^{+2} ion concentration of 400 ppm and then adjusted for each solution to optimum pH adsorption. Subsequently, (20 mg of GO or reduced size of GO) was added into each bottle. Samples were agitated of 60 min into a water bath sonicator at three different temperatures i.e. 25°C, 45°C, and 65°C. After that filtrate was separated by suction filtration. Ni (II) ion concentration was determined spectrophotometrically by measuring the absorbance of each solution at 393nm.

To obtain the isotherms of adsorption, eight different concentrations of Ni^{+2} were prepared in the range of 200-900 ppm, their pH was adjusted to the optimum pH. After that, 3.0 mL of each solution was introduced into bottles, containing the optimum dose of GO-450 nm or GO-200 nm (20 mg). Bottles were agitated at the optimum contact time of 60 minutes at optimum a constant temperature of 25°C in a water bath sonicator. Samples were filtered by suction filtration; the concentration of Ni^{+2} was determined spectrophotometrically by measuring each solution's absorbance at 393 nm. A systematic methodology of this study is shown in Scheme 7.

Put 3.0 ml of Ni^{+2} solution in 6 bottles

Adjusted pH to optimum pH of adsorption

Add (GO-450 nm),(GO-200nm) 20 mg into each bottles

Agitated 25 °C, 45°C, and 65°C for 60 min

Filtrate analyzed for Ni^{+2}
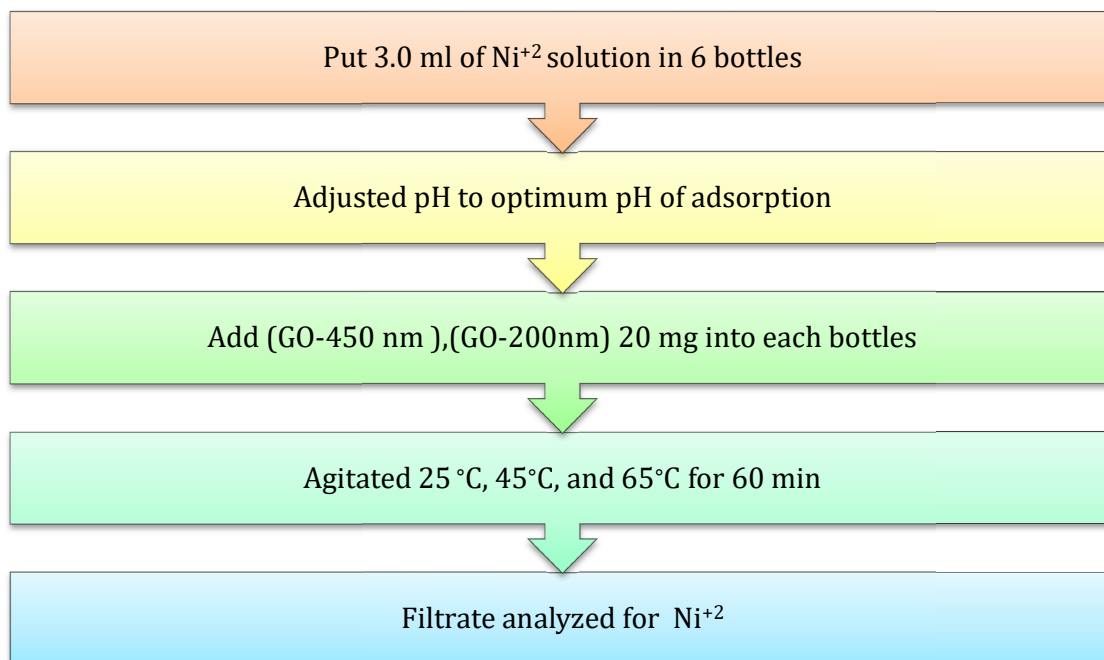
Scheme 6. *The systematic methodology of the temperature effect.*

Put 3.0 ml of different Ni^{+2} solution in 9 bottles

Adjusted pH to optimum pH of adsorption

Add (GO-450 nm),(GO-200 nm) 20 mg into each bottles

Agitated at 25 °c for 60 min

Filtrate analyzed for Ni^{+2}
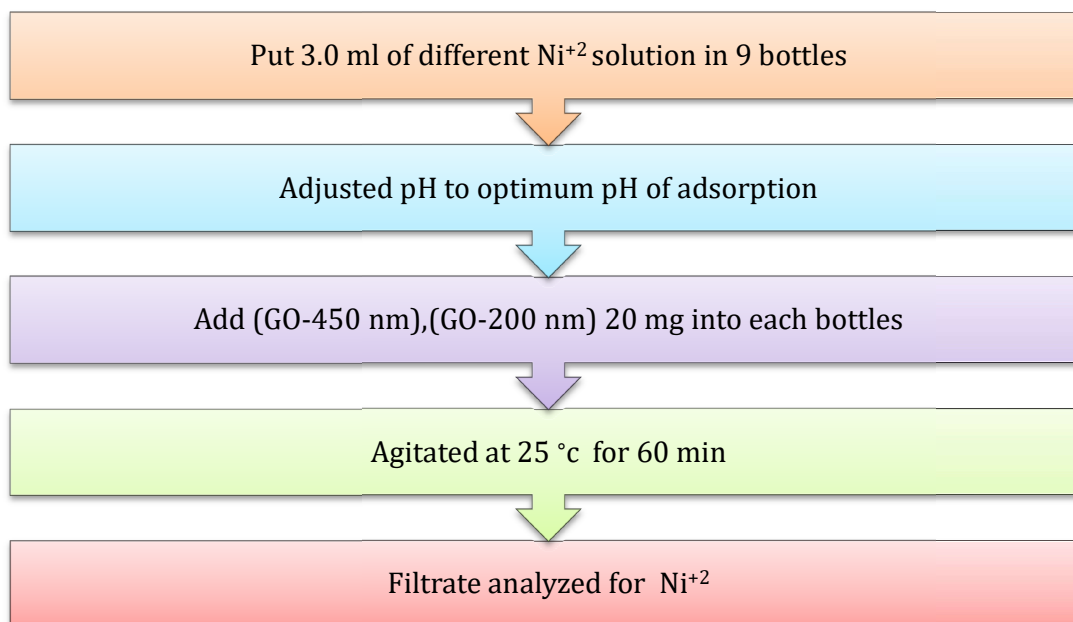
Scheme 7. *Systematic methodology of the initial concentration effect.*

Chapter Four:

Result and Discussion

4. Result and Discussion

The present study concerned graphene oxide (GO) synthesis and investigated the removal of nickel (II) ions by using two sizes of graphene oxide nanoparticles (GO-450 nm and GO-200 nm). The results obtained will be discussed under the following headings:

4.1 Characterization

4.1.1 Scanning Electron Microscopy (SEM)

The morphology and the lateral sizes of GO nanosheet were studied by scanning electron microscopy (SEM) [82, 84] Figure 9, SEM exhibits two sizes of graphene oxide nanosheet; the average size (lateral width) of prepared GO sheet is approximately 450 nm figure 9a. However, the average size of GO particles after sonication by using tip sonicator is approximately 200 nm Figure 9b.

Figure 9C represents the statistical analysis of GO particles deduced from SEM images.
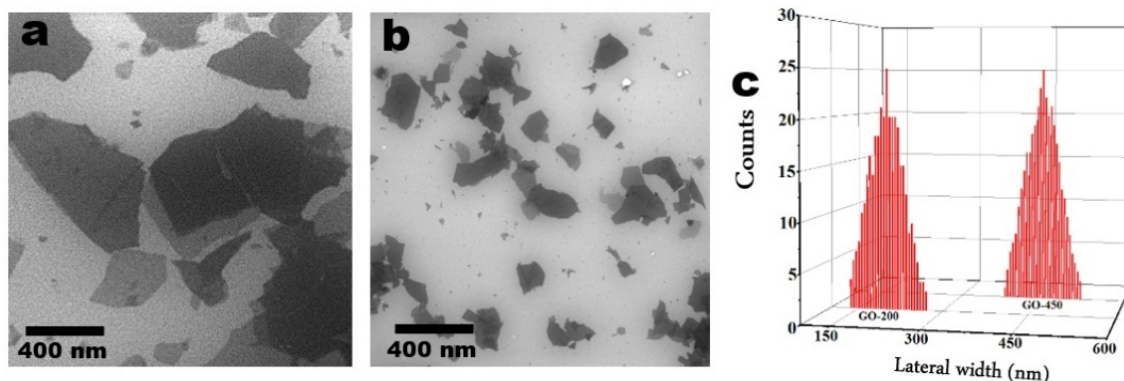
Figure 9. *SEM images of (a) GO-450 nm and (b) 200 nm. Panel (c) is the average width (nm) of GO particles deduced from SEM image, size distribution of GO-450 ± 35nm, GO-200 ± 20nm.*

4.1.2 FT-IR Study

The structure of graphite and graphite oxide (GO – 450nm) was studied by FTIR spectroscopy. The Graphite spectrum shows no notable bands in the region of the IR from 4000 cm^{-1} – 500 cm^{-1},however GO reveals variation bands at 3312, 1730, 1612, 1231, 1077 cm^{-1} corresponding to hydroxyl, carbonyl, -C=C-, epoxy, and C-O groups respectively figure 10a [78]. The broad band at 3312 cm^{-1} attributed to the stretching vibration of -OH group, which is due to the hydroxyl group of carboxylic acid at the edges of GO sheets as well as the alcohol groups distributed on the basal plane of graphene oxide layers. The significant peak at 1612cm^{-1} attributed to sp^2 hybridization on aromatic pattern -C=C-, and the peak appeared at 1730 cm^{-1} is due to C=O group. The weak band in the region of 1231 cm^{-1} is assigned to stretching vibration of epoxide group -CO, and the peak at 1077 cm^{-1} is due to the alkoxy group -C-O [35, 63]. Figure 10 b shows that the FTIR spectra of free Ni^{+2}, GO – Ni^{+2}, and GO – 200nm. Ni^{+2} in its compound which reveals a broad peak at 3200 cm^{-1} assigned to symmetric stretching of the water hydration , in addition to the bending vibration of water hydration observed at 1656 cm^{-1}. The other peaks at 1096 cm^{-1}, 465 cm^{-1}, 632 cm^{-1} ,and 797 cm^{-1} are corresponding to fundamental vibrations of SO$_4^{-2}$ ion namely as a non-degenerate, doubly degenerate, triply degenerate mode respectively. After adsorption of Ni^{+2}, the broad band at 3312 cm^{-1} ^{1}that is results from the stretching vibration of -OH group at the surface of GO was shifted to 3150 cm^{-1}. Moreover, the strong peak at 1730 cm^{-1} in C=O group shifted to 1715 cm^{-1} this findings indicate that Ni^{+2} adsorbed on GO particles. These findings are in agreement with previously reported data [79, 85].
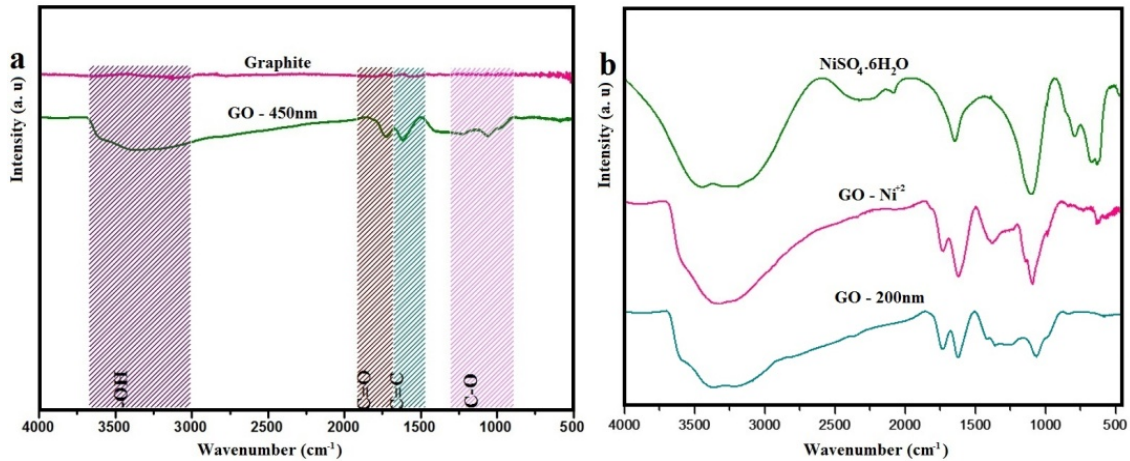
Figure 10. *FTIR spectra of (a) graphite and as prepared GO – 450 nm. (b) NiSO$_4$.6H$_2$O, GO – Ni^{+2} and GO – 200nm.*

4.1.3 UV-visible Spectrophotometer

In this study, UV-visible Spectrophotometer was used to determine the concentration of Ni^{+2} in their solution. The main principle of this instrument is depened on the amount of radiation at specific wavelength that absorbed by the particle (Ni^{+2}) in the solution. As the Ni^{+2}concentration increases, the absorbance increases as shown in Figure 11a. The absorption of radiation by Ni^{2+}is occurred at three different wavelengths; 393nm, 656nm, and 720nm .These wavelengths are assigned to:

$$\upsilon_1 = {}^3A_2g\ (F) \rightarrow {}^1Eg$$

$$\upsilon_2 = {}^3A_2g\ (F) \rightarrow {}^3T_1g\ (F)$$

$$\upsilon_3 = {}^3A_2g\ (F) \rightarrow {}^3T_1g\ (P).$$

The observed bands of 393 nm and 720 nm related to υ_3 and υ_2 respectively, while υ_1 refers to 656 nm [87].

Ni^{+2} solution of 400 ppm has been used to determine $\lambda\,max$ (maximum absorption wavelength). And it was equal 393 nm. Thus, the adsorption of all Ni^{2+} in their solutions

46

with a concentration between 0 and 900 ppm was determined at 393 nm, and the calibration

curve was plotted between absorbance and concentration of Ni^{+2} as shown in Figure 11a.
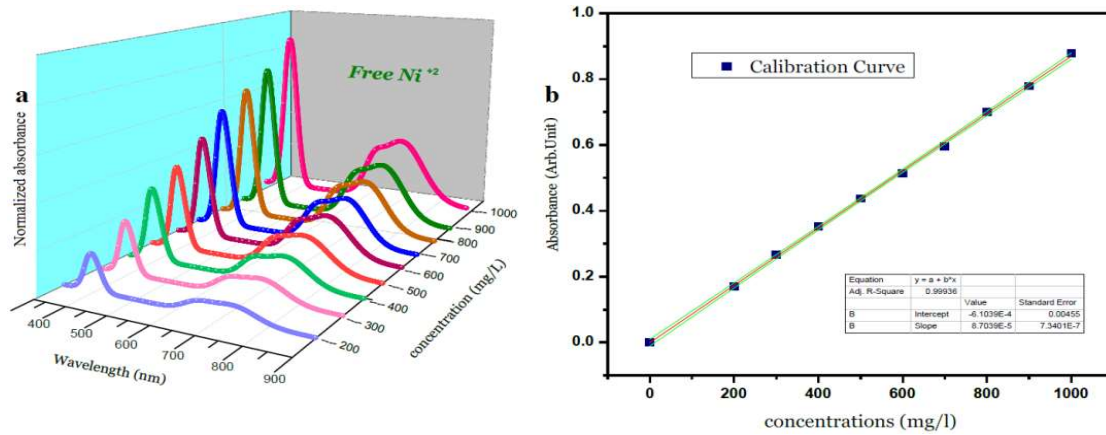
Figure 11. *(a) UV-visible spectroscpy of Ni^{+2} at different concentrations. (b) the calibration curve of Ni^{+2} samples.*

4.2 Adsorption Capacity

The adsorption capacity ($q_e, mg/g$) at different time intervals is increased with increasing

the initial Ni^{+2} concentrations as shown in figure 12. Moreover, the adsorption capacity of

GO sheets increased with decreasing GO lateral width. As shown in figure 12 a, the

adsorption capacity of GO– 450 nm appeared as stabilized behavior above 400 ppm Ni^{+2}

concentration. However, in figure 12 b the GO–200 nm exhibits a linear behavior with

increasing Ni^{+2} concentrations up to 900 ppm after 60 min of incubation, at 25°C and pH 6.
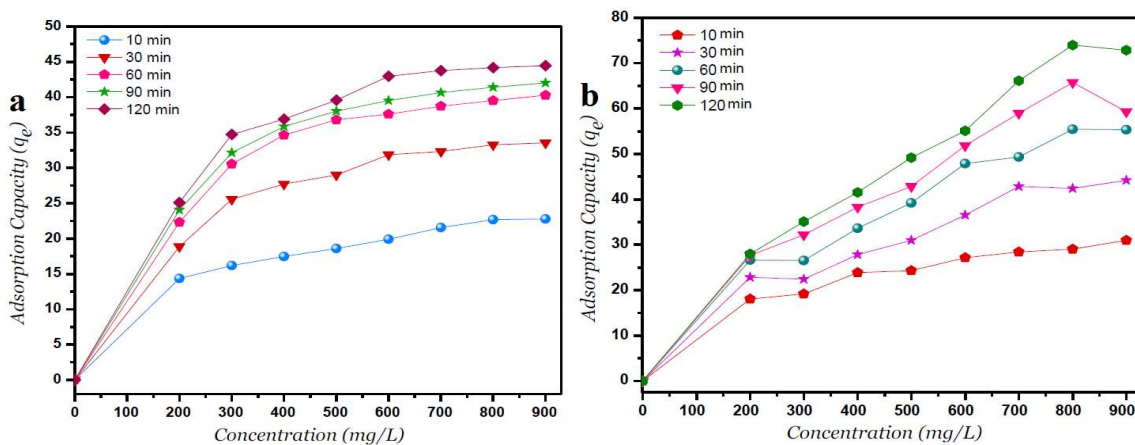
Figure 12. *Adsorption capacity versus Ni^{+2} concentrations for (a) GO-450nm and (b) GO – 200 nm at different time intervals.*

47

4.3 Percent Removal of Ni^{+2} at Different Concentrations and Time Intervals

Figure 13 shows the percent removal of Ni^{+2} ions is size dependent on the lateral width of GO sheets. As the size of GO decreased the percent removal of Ni^{+2} is increasing due to high surface areas of GO–200 nm. As shown in Figure 13a the contact time reveals a minor change on the removal of Ni^{+2} after 60 min of incubation. In panel (b) the size of GO sheets (GO – 200 nm) shows higher removal of Ni^{+2} due to increasing adsorbent surfaces [14, 35].
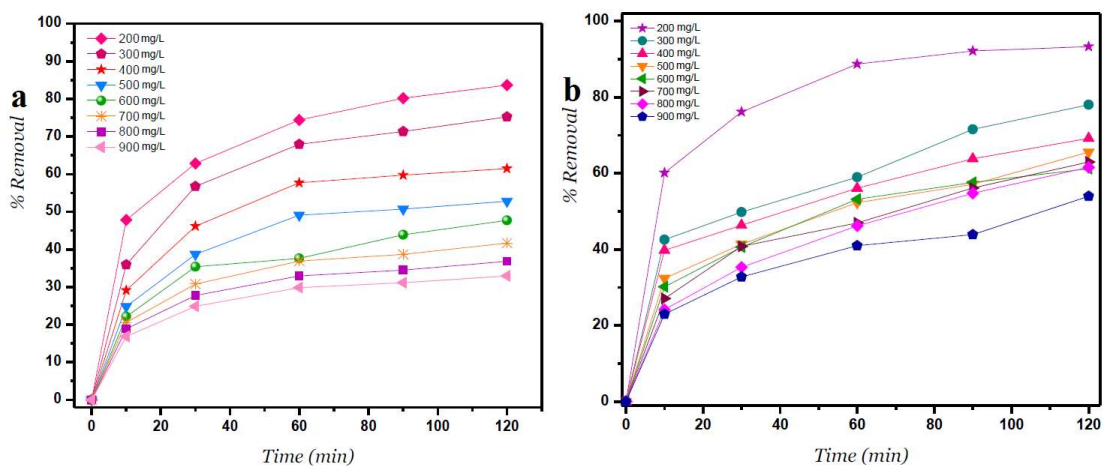
Figure 13. *The percent removal of Ni^{+2} onto (a) GO – 450 nm and (b)GO – 200 nm at different time intervals, T = 25 ^{0}C.*

4.4 pH Study

The pH profile indicated that the increasing of pH from 2 to 6 lead to drastically increasing on adsorbtion of Ni^{+2} onto the surface of GO –450 nm and GO – 200 nm, after pH 6, the adsorption of Ni^{+2} slightly increased with elevated pH until a pH of 10 as shown in figure 14 . Therefore, the optimum pH would be consider at 6.0 and will be used for further invistigation at this study.

This indicates that the competitive adsorption between Ni^{+2} ions and H_3O^+ ions on the surface of GO at pH higher than 6, the negative charge on the surface of GO particles increases and lead to strong electrostatic interaction between Ni^{+2} and GO particles under alkaline condition [25, 35]. On the other hand, Ni^{+2} ions can present as ($Ni(OH)^+$, $Ni(OH)_2$, $Ni(OH)_3^-$, $Ni(OH)_4^{-2}$) and this may lead to precipitation onto the surface of GO particles [79, 87].

The lateral sheet dimension (GO–200 nm) shows higher removal comparing with GO–450 nm. This behavior is attributed to more surfaces of GO particles.
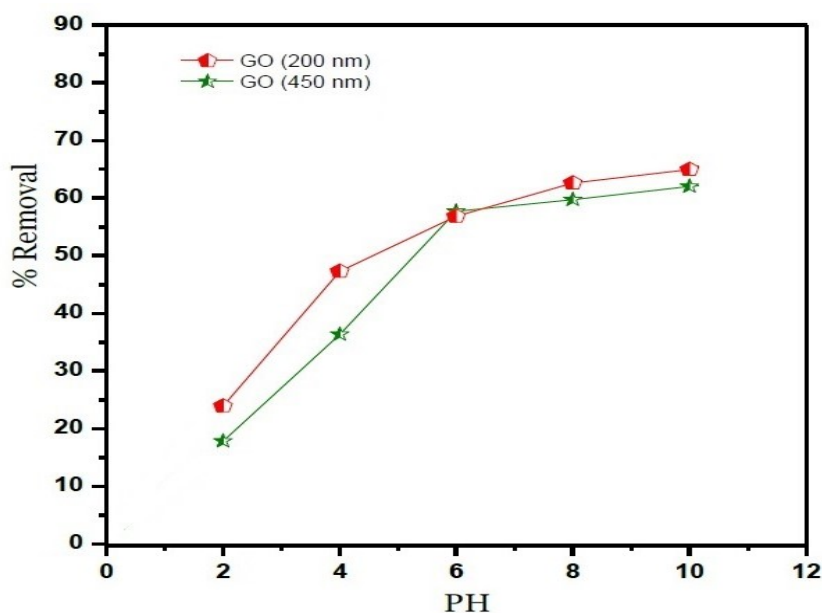
Figure 14. *Percent removal of Ni^{+2} at different pH values. Ni^{+2}= 400 ppm,   T= 25 ^{0}C.*

4.5 Adsorbent Dose

The effect of adsorbent dose on Ni^{+2} removals is shown in figure 15. The amount of GO varying from 1.0 to 80 mg, the initial concentration of Ni^{+2} was fixed at 400 ppm. The results reveal that the removal of Ni^{+2} by GO–450 nm increased drastically with increasing adsorption dose from 1.0 mg to 20 mg. This behavior is attributed to the increasing in the availability of surfaces at a higher amount of adsorbents. Thereafter, the adsorption is

increasing smoothly with increased the adsorbent dose from 20 mg to 80 mg. and this may

be imputed to overcrowding in the adsorbed molecules [14].
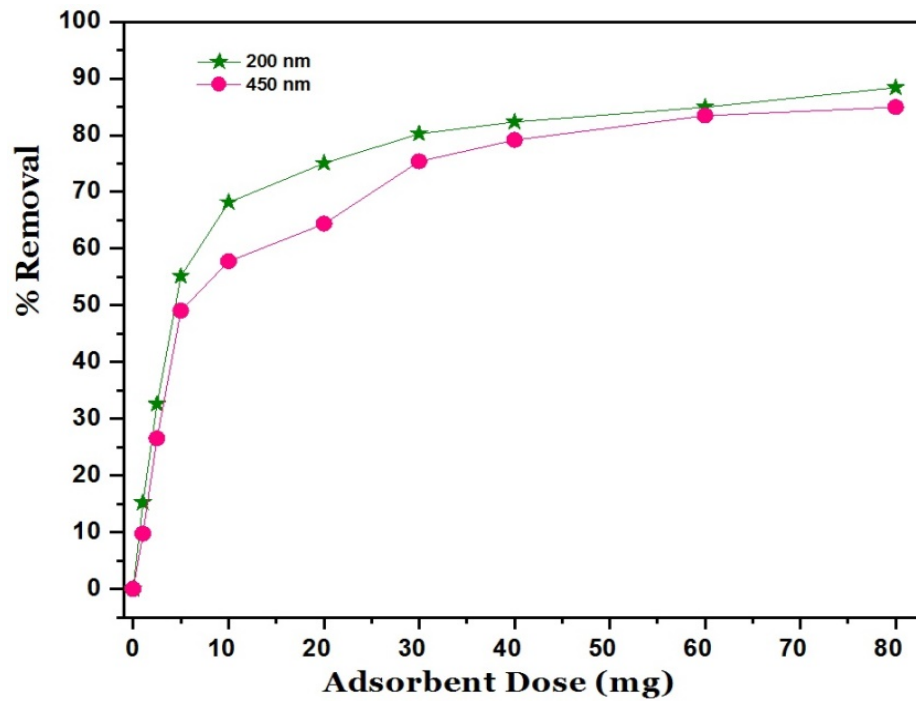
Figure 15. *Effect of adsorbent dose (Ni^{+2}= 400 ppm, T=25^{0}C, pH=6).*

4.6 Adsorption Isotherm Models

At uniform surrounding conditions, adsorption isotherms are used to correlate the mass of adsorbed material per unit of the mass of the adsorbent. The initial Ni^{+2} concentration was varied to model the adsorption isotherms where other parameters, which involve contact time, temperature, graphene oxide dose, pH, were kept fixed. Two different isotherms were used to fit the equilibrium data (see section 2.2.1.):

Langmuir isotherm (Equation 4).

Freundlich isotherm (Equation 7).

4.6.1 Langmuir Isotherm

Figure 16a, 17a presents the Langmuir adsorption isotherm of the Ni^{+2} by graphene oxide (450 nm and 200 nm), respectively at 25°C. The linear relation between C_e/q_e versus Ni^{+2} concentrations at equilibrium for different time intervals showed in figure 16 (a) at 450nm, panel (a) in figure17 at 200 nm. From these plots, the value of q_m and K_L was calculated and recorded in Table 7, and table 8. q_m values of Ni^{+2} onto GO–200 nm is higher than that for GO– 450 nm. This result indicated that a complete and uniform monolayer of Ni^{+2} covering the surfaces of GO particles over the whole concentrations. However, no final conclusion can be reached until further models of isotherms are examined.

4.6.2 Freundlich Isotherm

The Freundlich isotherm model interpreted as sorption to heterogeneous surfaces as shown in figure 16b. The Freundlich constant n between 1 and 10 provides favorable adsorption tends. The larger value of n means stronger interaction between the Ni^{+2} ions and GO nanoparticles as shown in table 7 and table 8. The Freundlich isotherm parameter (K_F) was calculated according to Equation 7, the value increases as the time interval increased which

indicates the Freundlich model fitted well with the experimental data. The correlation coefficient of Freundlich isotherm (R^2) was approximately 0.910.

Panel (b) in figure 17, the same linear relation appeared between $ln q_e$ versus $ln C_e$ for Freundlich isotherm. The value of n is higher than 1 indicated that the adsorption capacity was slightly restrained at lower equilibrium concentration. As shown in table 8, the values of n are studied as an indication of the linearity deviation, as well as it is used to predict the heterogeneity degree of the adsorbent. Moreover, the value of n is considered as an indication of whether the adsorption process is favorable or not. The value of n corresponding to GO–450 nm is greater than that with GO–200 nm, illustrating that a stronger capacity of Ni^{+2} onto GO–450 nm. The Freundlich constant K_F has been found as a relative measure of adsorption capacity. As the value of K_F increases the adsorption capacity increases. The reported values of K_F by using GO–450 nm as adsorbent was greater than that using GO– 200nm. This result summarizing that the uptake of Ni^{+2} ions with a high adsorption capacity of the adsorbent.
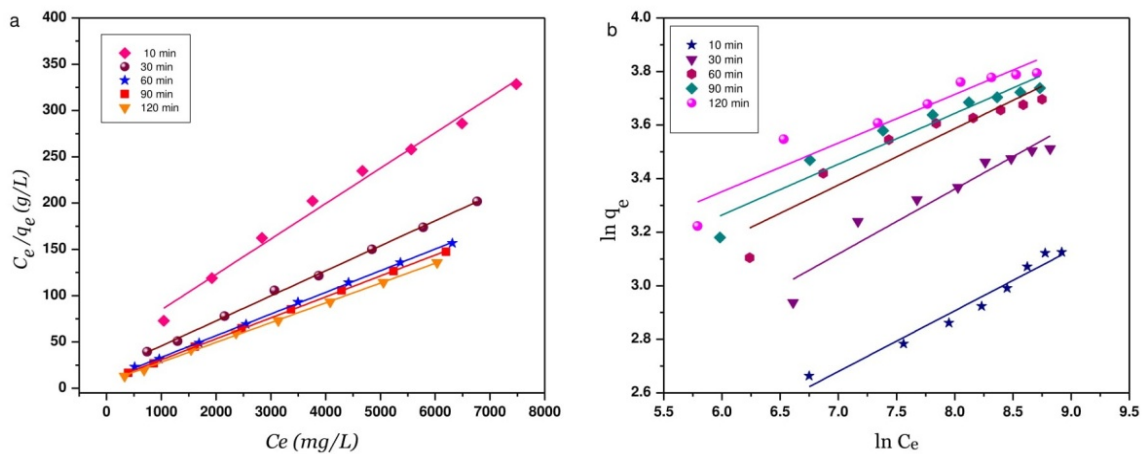
Figure 16. *Langmuir (a) and Freundlich (b) adsorption isotherm of Ni^{+2} onto GO – 450 nm at 25^0C.*
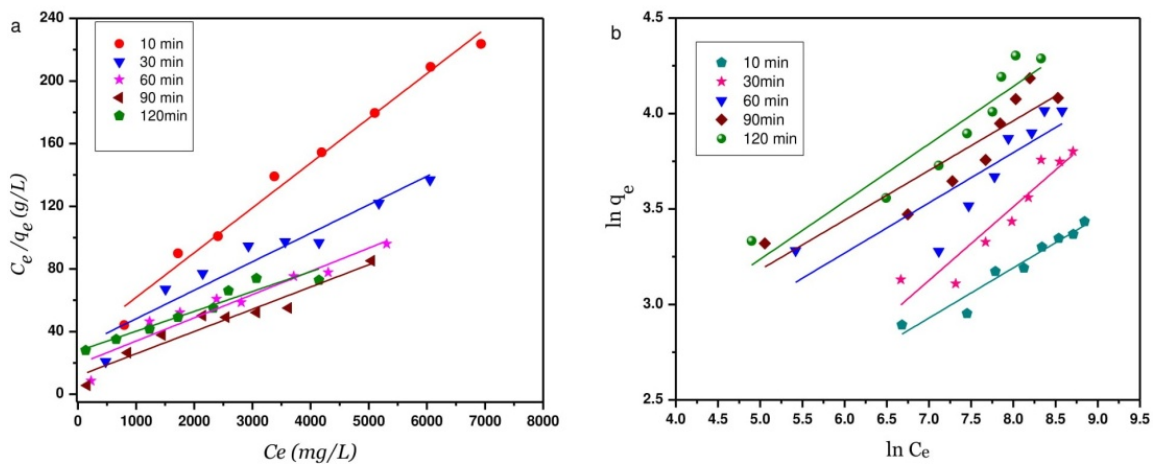
Figure 17. *Langmuir (a) and Freundlich (b) adsorption isotherm of Ni^{+2} onto GO – 200 nm at 25 ^{0}C.*

Table 7. Langmuir and Freundlich parameters for the adsorption of Ni^{+2} onto GO – 450 nm at 25 ^{0}C

Time (min)	Langmuir isotherm				Freundlich isotherm		
	q_m (mg .g^1)	K_L (L.mg^{-1})	R_L	R^2	K_F	n	R^2
10	26.316	0.0008	0.122	0.987	2.983	4.405	0.957
30	37.037	0.0014	0.074	0.998	4.149	4.132	0.912
60	43.478	0.0023	0.046	0.999	6.686	4.762	0.872
90	43.487	0.0028	0.036	0.999	8.381	5.291	0.919
120	46.729	0.0031	0.034	0.998	9.593	5.495	0.900

Table 8. Langmuir and Freundlich parameters for the adsorption of Ni^{+2} onto GO 200 nm at 25^{0}C

Time (min)	Langmuir isotherm				Freundlich isotherm		
	q_m (mg .g^1)	K_L (L.mg^{-1})	R_L	R^2	K_F	n	R^2
10	34.483	0.0008	0.113	0.985	2.968	3.802	0.936
30	55.556	0.0006	0.156	0.907	1.532	2.591	0.870
60	66.667	0.00078	0.124	0.901	5.419	3.802	0.709
90	71.428	0.0012	0.085	0.923	6.567	3.861	0.805
120	76.923	0.00047	0.191	0.916	5.624	3.311	0.869

In this work, the data of Ni^{+2} onto GO–450 nm and GO–200 nm of equilibrium adsorption was better described by the Langmuir adsorption isotherm model. The maximum adsorption capacities of monolayer were 43.478 mg/g and 66.667 mg/g for GO–450 nm and GO–200 nm respectively as shown in figure 18, and the isotherm parameters are summarized in Table 9.
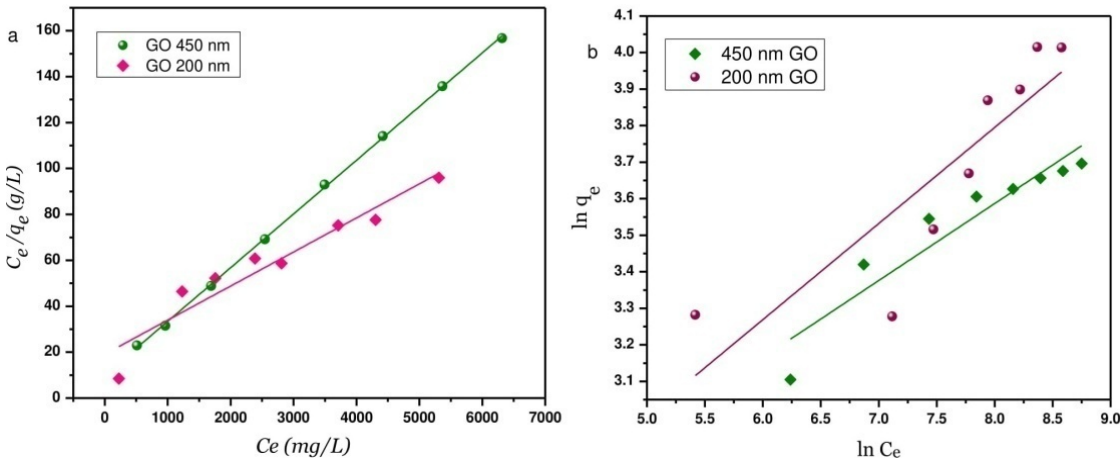
Figure 18. *Langmuir (a) and Freundlich (b) adsorption isotherm of Ni^{+2} onto 450 nm and 200 nm at 60 min of incubation.*

Table 9. Isotherm parameters and regression coefficient (R^2) of the models for GO (450 nm, 200 nm).

Adsorbent	Langmuir				Freundlich		
	$q_m(mg/g)$	$k_l(L/mg)$	R_L	R^2	n	K_f	R^2
GO 450nm	43.478	0.0023	0.046	0.999	4.762	6.686	0.872
GO 200nm	66.667	0.0008	0.124	0.901	3.802	5.419	0.709

4.7 kinetic Study

Understanding the kinetics of the adsorption process is important as this will help to scale this system up. In the literature, different predictive models are available to show the performance of the adsorption process when the contact time between the adsorbent and the adsorbate is varied. The pseudo-first-order (Lagergen model) and pseudo-second-order kinetics were used in this study using data from the experimental results (see Section 2.2.2).

Pseudo-first-order (Lagergen model) (Equation 9).

Pseudo-second-order (Ho's model) (Equation 11).

4.7.1 Pseudo-First-Order (Lagergen Model)

Figure 19a and figure 20a below shows the fitted Lagergren model experimental data, and it is apparent from the R^2 values that this model has a low variable response variation, and therefore, it cannot be used for predicting kinetic data. In addition, it displays non-linearity behavior and this verifies data scattering out of linear range.

4.7.2 Pseudo-Second-Order (Ho's model)

The R^2 in Figure 19 b and figure 20 b is high, and it means that this model can describe the variation in the response variable. The model also exhibited a linear trend with excellent data fit. This imposes that the experimental data fits into the kinetic model of the pseudo-second-order.
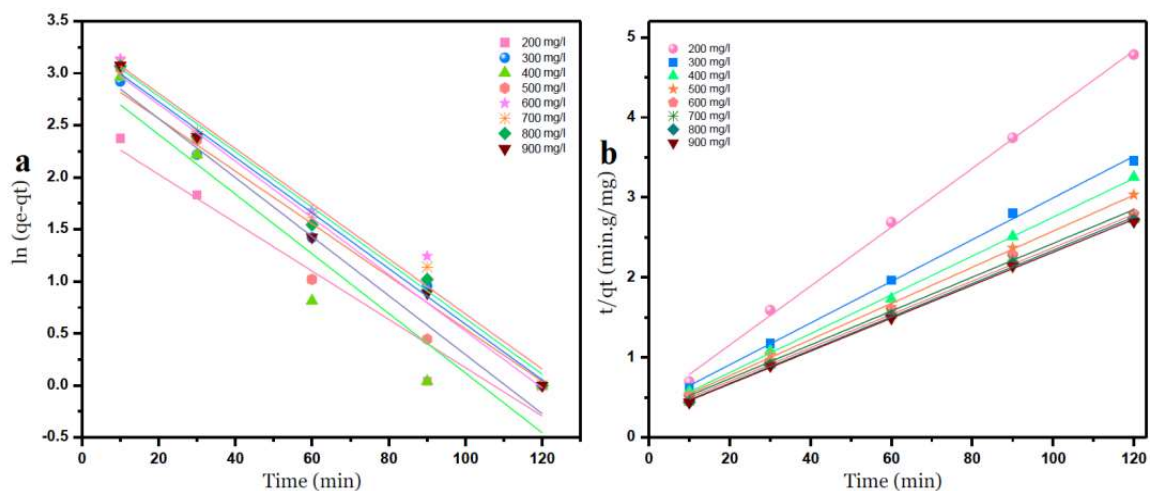
Figure 19. *Pesudo-first order (a) and Pseudo-second order (b) kinetic adsorption model of Ni^{+2} onto GO – 450 nm at 25 ^{0}C.*
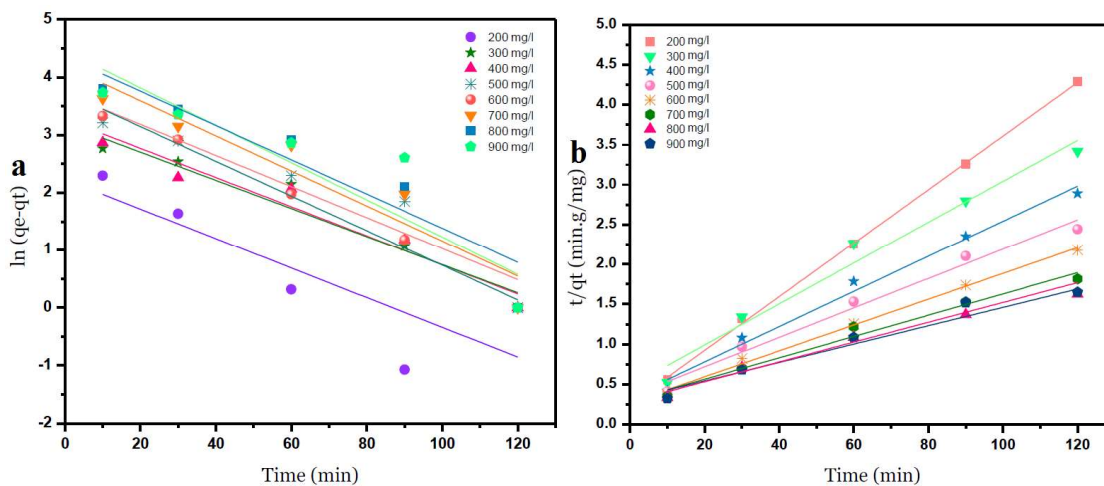
Figure 20.*Pseudo-first order (a) and Pseudo-second order (b) kinetic adsorption model of Ni^{+2} onto GO – 200 nm at 25 ^{0}C.*

The intercepts and slope of the linear plots for the adsorption of nickel by GO–450 nm and GO–200 nm were used to calculate the kinetic parameters, as shown in figure 21; the kinetic constant values are summarized in table 12.
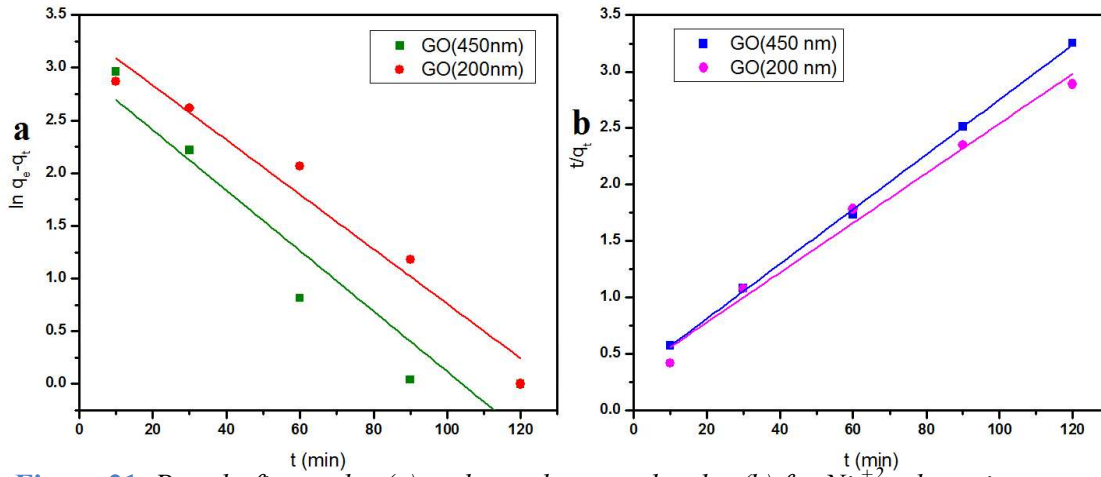
Figure 21. *Pseudo-first order (a) and pseudo-second order (b) for Ni^{+2} adsorption onto GO – 450 nm and GO – 200 nm. Ni^{+2}=400 ppm, T=25 ℃,   pH = 6.*

Table 10.pseudo-first-order and pseudo-second-order parameters for the adsorption of the Ni^{+2} onto GO – 450 nm at 25 ^{0}C.

C_i mg/l	$q_{e,exp}$ mg/g	Pseudo first- order			Pseudo-second order		
		K_1 min^{-1}	$q_{e,cal}$ mg/g	R^2	K_2 $g/mg.min$	$q_{e,cal}$ mg/g	R^2
200	25.093	0.023	12.098	0.929	0.00325	27.027	0.998
300	34.718	0.025	21.499	0.983	0.00147	38.462	0.998
400	36.889	0.029	19.747	0.883	0.00177	41.667	0.999
500	39.571	0.028	22.874	0.939	0.00645	43.478	0.999
600	42.963	0.027	28.106	0.968	0.00141	47.619	0.997
700	43.747	0.027	27.495	0.981	0.00153	47.619	0.998
800	44.183	0.028	26.076	0.987	0.00168	47.619	0.998
900	44.447	0.027	25.636	0.987	0.00171	47.619	0.999

59

Table 11.pseudo-first-order and pseudo-second-order parameters for the adsorption of the Ni^{+2} onto GO – 200 nm at 25 ^{0}C.

C_i mg/l	$q_{e,exp}$ mg/g	Pseudo first- order			Pseudo-second order		
		K_1 min^{-1}	$q_{e,cal}$ mg/g	R^2	K_2 $g/mg.min$	$q_{e,cal}$ mg/g	R^2
200	27.989	0.026	9.281	0.632	0.00459	29.412	0.999
300	35.105	0.025	26.469	0.930	0.00142	38.462	0.967
400	41.534	0.026	28.588	0.949	0.00143	45.455	0.983
500	49.164	0.027	41.470	0.867	0.00092	55.556	0.976
600	55.079	0.030	42.479	0.989	0.00095	62.500	0.994
700	66.137	0.030	66.819	0.861	0.00057	76.923	0.974
800	73.937	0.032	86.747	0.867	0.00046	83.330	0.971
900	72.825	0.029	77.029	0.741	0.00051	83.330	0.957

The value of the regression coefficient (R^2) of the pseudo-second-order model for GO–450 nm and GO–200nm is higher than pseudo-first-order. Also, the value of (q_e calculated = 41.667 and 45.455) from the pseudo-second-order for GO–450 nm and GO–200 nm are similar values of experimental adsorption capacity ($q_{e.exp}$ = 36.889 and 41.534), these results indicate that the nickel adsorption on GO–450 nm and GO–200 nm is the pseudo-second-order model.

Table 12. Kinetic Parameters and regression coefficient R^2 of Nickel adsorption on GO (450 nm, 200 nm).

Absorbent	$q_{e\ exp\ (mg/g)}$	Pseudo-first-order model			Pseudo-second-order model		
		$K_1(1/min)$	$q_{e\ cal\ (mg/g)}$	R^2	$K_2(1/min)$	$q_{e\ exp\ (mg/g)}$	R^2
GO 450nm	36.889	0.029	19.747	0.883	0.0018	41.667	0.999
GO 200nm	41.534	0.026	28.588	0.940	0.0014	45.455	0.983

4.8 Effect of Temperature

Understanding the thermodynamic behavior of the adsorption process is significant, and this can be done by calculating thermodynamic parameters that include enthalpy, entropy, and Gibbs free energy.

The linear relation between $ln(qe / Ce)$ and $1/T$ as shown in figure 22, with the slope reading the apparent enthalpy change. The calculated thermodynamic parameters using equations 12-13 (see section 2.2.3). [22, 88].
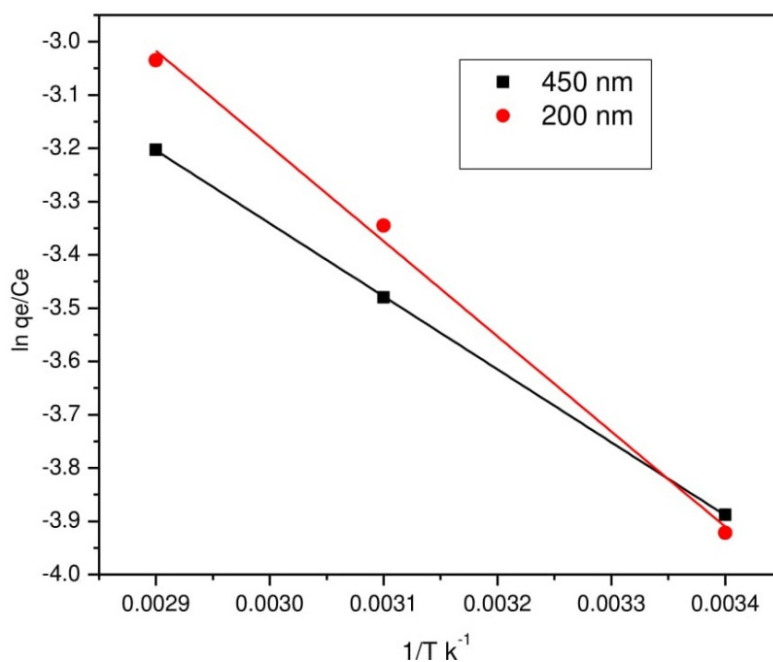
Figure 22. *Van't Hoff for the adsorption of Ni^{+2} onto 450 nm and 200 nm GO (Ni^{+2}=400 ppm).*

Changing the standard free energy decreases with rising temperatures regardless of the adsorbent nature. This indicates that higher temperatures actually provide better adsorption [22]. The adsorption range of free energy values ($\Delta G°$) is usually between -20.0 to 0 kJ/mol while the chemisorptions range of free energy values is between -80.0 and -400 kJ/mol. the negative values of $\Delta G°$ suggest that the adsorption of Ni^{+2} onto GO–450 nm

and 200 nm is a spontaneous process but as these values are in the range between -20 and 0 kJ/mol the process is classified physisorption. The positive values of ΔH° indicate that the adsorption process of Ni^{+2} onto GO–450 nm and 200 nm is an endothermic process while the positive values of ΔS° indicate that increased the randomness at the solid/liquid interface during the adsorption process, the thermodynamic parameters are presented in table 13 [90].

Table 13.Thermodynamic parameters for the adsorption of Ni^{+2} onto GO –450 and 200 nm.

Adsorbent	ΔH° kJ/mol	ΔS° J/mol.K	ΔG° kJ/mol		
			25 ^{0}C	45^{0}C	65^{0}C
GO – 450 nm	1.369	6.377	- 0.5311	- 0.6587	- 0.7862
GO – 200 nm	1.786	17.975	- 3.565	- 3.924	- 4.283

Chapter Five:

Conclusion and Recommendations

5.1 Conclusion

Due to their high toxicity and non-biodegradability, heavy metals are major inorganic pollutants. Tremendous use of heavy metals has resulted in an increased flux of metallic substances into the aquatic environment over the past few decades. Due to its promising properties, graphene oxide (GO) has gained renewed interest in the technologically anchored, modern society. The removal of heavy metal ions from aqueous solution can be achieved by using graphene oxide particles at different size distributions (GO–450 nm and GO– 200 nm). The smaller size of GO particles provided better removal due to high surface to volume ratio, as well as various oxygen groups like hydroxyl, epoxy, and carboxyl present after oxidation and ultrasonication. The adsorption capacity of GO–450 nm appeared as stabilized behavior above 400 mg/l Ni^{+2} concentrations. However the GO– 200 nm exhibits a linear behavior with increasing Ni^{+2} concentrations up to 900 mg/L after 60 min of incubation. This research demonstrates that GO particles can be an effective adsorbent for toxic metal removal.

5.2 Recommendations

Further studies will be carried out graphene oxide to enhance the functional group on its surface either by coated it with by using different oxides or composite oxides such as (MnO_2, Al_2O_3, Fe_2O_3, TiO_2, and Fe_3O_4), or by advanced oxidation step to increase the carboxylic group on its surface, in turn, increase the adsorption site and affinity on graphene oxide, moreover, a real sample from polluted water with nickel will be introduced to treat it.

References

[1] T. J. Booth and M. A. B. Baker, *Nanotechnology: Building and Observing at the Nanometer Scale*. Elsevier Inc., 2016.

[2] S. Bhattacharya, I. Saha, A. Mukhopadhyay, D. Chattopadhyay, and U. Chand, "Role of Nanotechnology in Water Treatment and Purification: Potential Applications and Implications," *Int. J. Chem. Sci. Technol.*, vol. 3, no. 3, pp. 59–64, 2013.

[3] A. R. and J. Bhattacharya, *Nanotechnology in Industrial Wastewater Treatment*, vol. 13. IWA Publishing, 2014.

[4] T. Ada and R. Contreras Rodríguez, "Removal of Cadmium (II), Lead (II) and Chromium (VI) in Water with Nanomaterials," 2015.

[5] X. Qu, P. J. J. Alvarez, and Q. Li, "Applications of Nanotechnology in Water and Wastewater Treatment," *Water Res.*, vol. 47, no. 12, pp. 3931–3946, 2013.

[6] P. Xu *et al.*, "Use of Iron Oxide Nanomaterials in Wastewater Treatment: A review," *Sci. Total Environ.*, vol. 424, pp. 1–10, 2012.

[7] F. C. Adams and C. Barbante, "Nanoscience, Nanotechnology and Spectrometry," *Spectrochim. Acta - Part B At. Spectrosc.*, vol. 86, pp. 3–13, 2013.

[8] A. Lele, "Role of Nanotechnology in Defence," *Strateg. Anal.*, vol. 33, no. 2, pp. 229–241, 2009.

[9] T. Ahmed, S. Imdad, K. Yaldram, N. M. Butt, and A. Pervez, "Emerging Nanotechnology-Based Methods for Water Purification: A review," *Desalin. Water Treat.*, vol. 52, no. 22–24, pp. 4089–4101, 2014.

[10] S.-H. A. S. A. Lens, J.Virkutyte, V.Jegatheesan, *Nanotechnology for Water and Waste Water Treatment*. 2018.

[11] K. Padmaja, J. Cherukuri, and M. A. Reddy, "Conventional to Cutting Edge Technologiesin Drinking Water Purification - A Review," *Int. J. Innov. Res. Sci. Eng. Technol.*, vol. 3, no. 1, pp. 9375–9385, 2014.

[12] J. Brame, Q. Li, and P. J. J. Alvarez, "Nanotechnology-Enabled Water Treatment and Reuse: Emerging Opportunities and Challenges for Developing Countries," *Trends Food Sci. Technol.*, vol. 22, no. 11, pp. 618–624, 2011.

[13] J. Theron, J. A. Walker, and T. E. Cloete, "Nanotechnology and Water Treatment: Applications and Emerging Opportunities," *Crit. Rev. Microbiol.*, vol. 34, no. 1, pp. 43–69, 2008.

[14] W. Konicki, M. Aleksandrzak, and E. Mijowska, "Equilibrium and Kinetics Studies for the Adsorption of Ni^{2+} and Fe^{3+} Ions from Aqueous Solution by Graphene Oxide," *Polish J. Chem. Technol.*, vol. 19, no. 3, pp. 120–129, 2017.

[15] P. C. Nagajyoti, K. D. Lee, and T. V. M. Sreekanth, "Heavy Metals, Occurrence and

Toxicity for Plants: A review," *Environ. Chem. Lett.*, vol. 8, no. 3, pp. 199–216, 2010.

[16] R. Goyer, F. United States. Environmental Protection Agency. Risk Assessment, and I. Eastern Research Group, "Issue paper on the human health effects of metals," 2004.

[17] A. Catenacci, "Heavy Metal Removal from Water: Charactarization and Applicability of Unconventional Media," School of Politecnico di Milano, 2014.

[18] S. SIMS, "Nickel Adsorption Studies on Synthesized Graphene Oxide and Magnetic Graphene Oxide," 2017.

[19] M. A. Barakat, "New Trends in Removing Heavy Metals from Industrial Wastewater," *Arab. J. Chem.*, vol. 4, no. 4, pp. 361–377, 2011.

[20] E. Ç. Salihi, J. Wang, D. J. L. Coleman, and L. Šiller, "Enhanced Removal of Nickel(II) ions from Aqueous Solutions by SDS-Functionalized Graphene Oxide," *Sep. Sci. Technol.*, vol. 51, no. 8, pp. 1317–1327, 2016.

[21] V. R. Kinhikar, "Removal of Nickel (II) from Aqueous Solutions by Adsorption with Granular Activated Carbon (GAC)," *Res. J. Chem. Sci.*, vol. 2, no. 6, pp. 6–11, 2012.

[22] S. M. Sallam, A. El-saharty, and A. Ahmed, "Adsorption of Toxic Ni (II) from an Aqueous Solution by Bentonite," *Int. J. Ecotoxicol. Ecobiol.*, vol. 2, no. 4, pp. 158–165, 2017.

[23] P. Tan, Y. Hu, and Q. Bi, "Competitive Adsorption of Cu^{2+}, Cd^{2+} and Ni^{2+} from an Aqueous Solution on Graphene Oxide Membranes," *Colloids Surfaces A Physicochem. Eng. Asp.*, vol. 509, pp. 56–64, 2016.

[24] F. Najafi *et al.*, "Thermodynamics of the Adsorption of Nickel Ions from Aqueous Phase Using Graphene Oxide and Glycine Functionalized Graphene oxide," *J. Mol. Liq.*, vol. 208, pp. 106–113, 2015.

[25] S. Mohamed Sallam, "Adsorption of Toxic Ni (II) from an Aqueous Solution by Bentonite," *Int. J. Ecotoxicol. Ecobiol.*, vol. 2, no. 4, p. 158, 2018.

[26] L. A. Chacra, "Treatment of Produced Water Using Graphene.," American University of Sharjah, 2016.

[27] V. H. Grassian, *Nanoscience and Nanotechnology*, no. July. 2004.

[28] J. L. Han *et al.*, "Shielding Membrane Surface Carboxyl Groups by Covalent-Binding Graphene Oxide to Improve Anti-Fouling Property and the Simultaneous Promotion of flux," *Water Res.*, vol. 102, pp. 619–628, 2016.

[29] K. Dermentzis, A. Christoforidis, and E. Valsamidou, "Removal of Nickel, Copper, Zinc and Chromium from Synthetic and Industrial Wastewater by Electrocoagulation," *Int. J. Environ. Sci.*, vol. 1, no. 5, pp. 697–710, 2011.

[30] C. Santhosh, V. Velmurugan, G. Jacob, S. K. Jeong, A. N. Grace, and A. Bhatnagar,

"Role of Nanomaterials in Water Treatment Applications: A review," *Chem. Eng. J.*, vol. 306, pp. 1116–1137, 2016.

[31] J. Xu *et al.*, "A review of Functionalized Carbon Nanotubes and Graphene for Heavy Metal Adsorption from Water: Preparation, Application, and Mechanism," *Chemosphere*, vol. 195, pp. 351–364, 2018.

[32] H. A. T. Amer, "Removal of Lead from Industrial Wastewater Using a Low Cost Waste Material," American University in Cairo, 2015.

[33] A. El Rahman and M. Gepreel, "Nanotechnology Applications in Water Treatment: Future Avenues and Challenges: A review," *6th Int. Perspect. Water Resour. Environ. Conf.*, no. December, 2013.

[34] C. P. Bergmann, *Carbon Nanomaterials as Adsorbents for Environmental and Biological Applications*. 2015.

[35] L. Prasanna, J. Reddy, H. Roh, Y. Choi, Y. Chang, and J. Yang, "Hydrometallurgy Adsorption Removal of Co (II) from Waste-Water Using Graphene Oxide," *Hydrometallurgy*, 2015.

[36] F. Perreault, A. Fonseca De Faria, and M. Elimelech, "Environmental Applications of Graphene-Based Nanomaterials," *Chem. Soc. Rev.*, vol. 44, no. 16, pp. 5861–5896, 2015.

[37] M. Kaur, "Nickel Adsorption Studies on Synthesized Graphene Oxide and Magnetic Graphene Oxide," Punjab Agricultural University, 2016.

[38] P. S. Karthik, A. L. Himaja, and S. P. Singh, "Carbon-Allotropes: Synthesis Methods, Applications and Future Perspectives," *Carbon Lett.*, vol. 15, no. 4, pp. 219–237, 2014.

[39] N. Saifuddin, A. Z. Raziah, and A. R. Junizah, "Carbon nanotubes: A review on Structure and Their Interaction With Proteins," *J. Chem.*, vol. 2013, 2013.

[40] M. Anjum, R. Miandad, M. Waqas, F. Gehany, and M. A. Barakat, "Remediation of Wastewater Using Various Nano-Materials," *Arab. J. Chem.*, 2016.

[41] Q. L. Yan, M. Gozin, F. Q. Zhao, A. Cohen, and S. P. Pang, "Highly Energetic Compositions Based on Functionalized Carbon Nanomaterials," *Nanoscale*, vol. 8, no. 9, pp. 4799–4851, 2016.

[42] A. D. Darwish, "Fullerenes," *Annu. Reports Prog. Chem. - Sect. A*, vol. 109, no. May 2015, pp. 436–452, 2013.

[43] G. UYAR, "A low-cost Adsorbent for Dye Removal: Methylene Blue Removal by Alginate-Montmorillonite Hybrid Beads," Istanbul Technical University, 2012.

[44] M. R. Servos, *Nanotechnology for Water Treatment and Purication Foreword by*. 2014.

[45] V. Gunarathne, A. Ashiq, and M. P. Ginige, *Green Adsorbents for Pollutant Removal*, vol. 18, no. May. 2018.

[46] A. Magrez *et al.*, "Cellular Toxicity of Carbon-Based Nanomaterials," *Nano Lett.*, vol. 6, no. 6, pp. 1121–1125, Jun. 2006.

[47] Y. Chang *et al.*, "In Vitro Toxicity Evaluation of Graphene Oxide on A549 Cells," *Toxicol. Lett.*, vol. 200, no. 3, pp. 201–10, Mar. 2011.

[48] E. L. K. Chng and M. Pumera, "The Toxicity of Graphene Oxides: Dependence on the Oxidative Methods Used," *Chem. - A Eur. J.*, vol. 19, no. 25, pp. 8227–35, Jun. 2013.

[49] Y. Cao and X. Li, "Adsorption of Graphene for the Removal of Inorganic Pollutants in Water Purification: A review," *Adsorption*, vol. 20, no. 5–6, pp. 713–727, 2014.

[50] W. Peng, H. Li, Y. Liu, and S. Song, "A review on Heavy Metal Ions Adsorption from Water by Graphene Oxide and its Composites," *J. Mol. Liq.*, vol. 230, pp. 496–504, 2017.

[51] L. Liu, X. B. Luo, L. Ding, and S. L. Luo, "Application of Nanotechnology in the Removal of Heavy Metal From Water," in *Nanomaterials for the Removal of Pollutants and Resource Reutilization*, Elsevier Inc., 2018, pp. 83–147.

[52] A. Khalid, M. Zubair, and Ihsanullah, "A Comparative Study on the Adsorption of Eriochrome Black T Dye from Aqueous Solution on Graphene and Acid-Modified Graphene," *Arab. J. Sci. Eng.*, vol. 43, no. 5, pp. 2167–2179, 2018.

[53] F. S. Awad, K. M. AbouZied, W. M. Abou El-Maaty, A. M. El-Wakil, and M. Samy El-Shall, "Effective Removal of Mercury(II) from Aqueous Solutions by Chemically Modified Graphene Oxide Nanosheets," *Arab. J. Chem.*, no. Ii, 2018.

[54] S. Bayu, "Investigation and Modeling of Cesium (I) Adsorption by Turkish Clays : Bentonite ," *Environ. Prog.*, vol. 30, no. 1, 2011.

[55] H. Qiu, L. Lv, B. C. Pan, Q. J. Zhang, W. M. Zhang, and Q. X. Zhang, "Critical Review in Adsorption Kinetic Models," *J. Zhejiang Univ. Sci. A*, vol. 10, no. 5, pp. 716–724, 2009.

[56] J. Y. Lim, N. M. Mubarak, E. C. Abdullah, S. Nizamuddin, M. Khalid, and Inamuddin, "Recent Trends in the Synthesis of Graphene and Graphene Oxide Based Nanomaterials for Removal of Heavy Metals — A review," *J. Ind. Eng. Chem.*, vol. 66, pp. 29–44, 2018.

[57] Y. Huang, X. Zeng, L. Guo, J. Lan, L. Zhang, and D. Cao, "Heavy Metal Ion Removal of Wastewater by Zeolite-Imidazolate Frameworks," *Sep. Purif. Technol.*, vol. 194, no. November 2017, pp. 462–469, 2018.

[58] J. He, S. Hong, L. Zhang, F. Gan, and Y. Ho, "Equilibrium and Thermodynamic Parameters of," *Fresenius Environ. Bull.*, vol. 19, no. 11, pp. 2651–2656, 2010.

[59] M. A. Ahmad, N. A. Ahmad Puad, and O. S. Bello, "Kinetic, Equilibrium and Thermodynamic Studies of Synthetic Dye Removal Using Pomegranate Peel Activated Carbon Prepared by Microwave-Induced KOH Activation," *Water Resour. Ind.*, vol. 6, pp. 18–35, 2014.

[60] N. M. Barkoula, B. Alcock, N. O. Cabrera, and T. Peijs, "Flame-Retardancy Properties of Intumescent Ammonium Poly(Phosphate) and Mineral Filler Magnesium Hydroxide in Combination with Graphene," *Polym. Polym. Compos.*, vol. 16, no. 2, pp. 101–113, 2008.

[61] M. Ahmaruzzaman, "Industrial Wastes as low-cost Potential Adsorbents for the Treatment of Wastewater Laden With Heavy Metals," *Adv. Colloid Interface Sci.*, vol. 166, no. 1–2, pp. 36–59, 2011.

[62] S. Iftekhar, D. L. Ramasamy, V. Srivastava, M. B. Asif, and M. Sillanpää, "Understanding the Factors Affecting the Adsorption of Lanthanum Using Different Adsorbents: A critical review," *Chemosphere*, vol. 204, pp. 413–430, 2018.

[63] W. Peng, H. Li, Y. Liu, and S. Song, "A review on Heavy Metal Ions Adsorption from Water by Graphene Oxide and its Composites," *J. Mol. Liq.*, vol. 230, pp. 496–504, 2017.

[64] M. Rao, A. V Parwate, and A. G. Bhole, "Removal of Cr^{6+} and Ni^{2+} from Aqueous Solution Using Bagasse and Fly Ash," vol. 22, pp. 821–830, 2002.

[65] Z. Gao, T. J. Bandosz, Z. Zhao, M. Han, and J. Qiu, "Investigation of Factors Affecting Adsorption of Transition Metals on Oxidized Carbon Nanotubes," vol. 167, pp. 357–365, 2009.

[66] S. Yang, J. Li, D. Shao, J. Hu, and X. Wang, "Adsorption of Ni (II) on Oxidized Multi-walled Carbon Nanotubes : Effect of Contact Time , pH , Foreign Ions and PAA," vol. 166, pp. 109–116, 2009.

[67] H. Hasar, "Adsorption of Nickel (II) from Aqueous Solution onto Activated Carbon Prepared from Almond Husk," vol. 97, pp. 49–57, 2003.

[68] Y. Ren *et al.*, "Graphene δ/MnO_2 Composite as Adsorbent for the Removal of Nickel Ions from Wastewater," *Chem. Eng. J.*, vol. 175, pp. 1–7, 2011.

[69] A. Ewecharoen, P. Thiravetyan, and W. Nakbanpote, "Comparison of Nickel Adsorption from Electroplating Rinse Water by Coir Pith and Modified Coir Pith," vol. 137, pp. 181–188, 2008.

[70] A. Kumar, G. K. Mishra, P. K. Rai, C. Rajagopal, and P. N. Nagar, "Removal of Heavy Metal Ions from Aqueous Solutions Using Carbon Aerogel as an Adsorbent," vol. 122, pp. 161–170, 2005.

[71] V. K. Gupta, A. Nayak, S. Agarwal, M. Chaudhary, and I. Tyagi, "Removal of Ni (II) Ions from Water Using Scrap Tire," *J. Mol. Liq.*, vol. 190, pp. 215–222, 2014.

[72] J. Hu, G. Chen, and I. M. C. Lo, "Selective Removal of Heavy Metals from Industrial Wastewater Using Maghemite Nanoparticle: Performance and Mechanisms," *J. Environ. Eng.*, vol. 132, no. 7, pp. 709–715, 2006.

[73] P. S. Kumar and K. Kirthika, "Equilibrium and Kinetic Study of Adsorption of Nickel from Aqueous Solution onto Bael Tree Leaf Powder," *J. Eng. Sci. Technol.*, vol. 4, no. 4, pp. 351–363, 2009.

[74] P. Parthasarathy and S. K. Narayanan, "Effect of Hydrothermal Carbonization Reaction Parameters," *Environ. Prog. Sustain. Energy*, vol. 33, no. 3, pp. 676–680, 2014.

[75] Y. C. Sharma, V. Srivastava, V. K. Singh, S. N. Kaul, and C. H. Weng, "Nano-adsorbents for the Removal of Metallic Pollutants from Water and Wastewater," *Environ. Technol.*, vol. 30, no. 6, pp. 583–609, 2009.

[76] A. Sheikhmohammadi *et al.*, "Application of Graphene Oxide Modified with 8-Hydroxyquinoline for the Adsorption of Cr (VI) from Wastewater: Optimization, Kinetic, Thermodynamic and Equilibrium Studies," *J. Mol. Liq.*, vol. 233, no. Vi, pp. 75–88, 2017.

[77] F. Najafi *et al.*, "Thermodynamics of the Adsorption of Nickel Ions from Aqueous Phase Using Graphene Oxide and Glycine Functionalized Graphene Oxide," *J. Mol. Liq.*, vol. 208, pp. 106–113, 2015.

[78] R. L. White, C. M. White, H. Turgut, A. Massoud, and Z. R. Tian, "Comparative Studies on Copper Adsorption by Graphene Oxide and Functionalized Graphene Oxide Nanoparticles," *J. Taiwan Inst. Chem. Eng.*, vol. 85, pp. 18–28, Apr. 2018.

[79] L. Liu *et al.*, "Talanta Preparation and Characterization of Chitosan / Graphene Oxide Composites for the Adsorption of Au (III) and Pd (II)," *Talanta*, vol. 93, pp. 350–357, 2012.

[80] E. Ç. Salihi, J. Wang, D. J. L. Coleman, and L. Šiller, "Enhanced Removal of Nickel (II) Ions from Aqueous Solutions by SDS-Functionalized Graphene Oxide," vol. 6395, no. March, 2016.

[81] G. Zhao *et al.*, "Removal of Pb(ii) Ions from Aqueous Solutions on Few-layered Graphene Oxide Nanosheets," *Dalt. Trans.*, vol. 40, no. 41, pp. 10945–10952, 2011.

[82] N. I. Zaaba, K. L. Foo, U. Hashim, S. J. Tan, W. W. Liu, and C. H. Voon, "Synthesis of Graphene Oxide using Modified Hummers Method: Solvent Influence," *Procedia Eng.*, vol. 184, pp. 469–477, 2017.

[83] S. Makharza *et al.*, "Graphene Oxide-Based Drug Delivery Vehicles: Functionalization, Characterization, and Cytotoxicity Evaluation," *J. Nanoparticle Res.*, vol. 15, no. 12, 2013.

[84] S. Makharza *et al.*, "Size-Dependent Nanographene Oxide as a Platform for Efficient Carboplatin Release," *J. Mater. Chem. B*, vol. 1, no. 44, pp. 6107–6114, 2013.

[85] O. Vittorio *et al.*, "Doxorubicin Synergism and Resistance Reversal in Human Neuroblastoma BE(2)C Cell Lines: An in Vitro Study With Dextran-catechin Nanohybrids," *Eur. J. Pharm. Biopharm.*, vol. 122, no. July 2017, pp. 176–185, 2018.

[86] P. Kathiravan, T. Balakrishnan, C. Srinath, K. Ramamurthi, and S. Thamotharan, "ScienceDirect Growth and Characterization of a -Nickel Sulphate Hexahydrate Single Crystal," *Karbala Int. J. Mod. Sci.*, 2016.

[87] Z. N. RAJAB, "Electronic Spectroscopy of Some Transition Metal Ion Compounds in A new Ionic Liquid," Al-Nahrain University, 2009.

[88] W. Konicki and E. Mijowska, "Equilibrium and Kinetics Studies for the Adsorption of Ni^{2+} and Fe^{3+} Ions from Aqueous Solution by Graphene Oxide," pp. 120–129, 2017.

[89] S. Maji *et al.*, "Efficiency Evaluation of Arsenic(III) Adsorption of Novel Graphene Oxide@Iron-aluminium Oxide Composite for the Contaminated Water Purification," *Sep. Purif. Technol.*, vol. 197, no. Iii, pp. 388–400, 2018.

[90] S. Patil, S. Renukdas, and N. Patel, "licensee IPA-Open access-Distributed under Creative Commons Attribution License 2.0 Removal of methylene blue, a basic dye from aqueous solutions by adsorption using teak tree (Tectona grandis) bark powder," *Int. J. Environ. Sci.*, vol. 1, no. 5, pp. 711–726, 2011.

المُلَخّص

تَمَّ دراسةِ إزالةِ أيوناتِ النيكل (II) في هذا البحث باستخدامِ جزيئاتِ أكسيدِ الغرافين (GO-450nm وGO-200nm) النانوية. سُمكُ صفيحةِ أكسيدِ الغرافين (GO) وأبعادُها الجانبيةِ تُعتبرُ مواداً ممتصةً مهمةً وأسلوباً واعداً لإزالةِ المعادنٍ كالنيكل والرصاص والنحاس بشكلٍ فعال. تم تحضيرُ أكسيدِ الغرافين (GO) عن طريقِ تفاعلِ التأكسدِ والاختزالِ(طريقة Hummer), كما وتم تسمية المنتجِ النهائيّ بأكسيدِ الغرافين GO-450nm. قمنا باستخدامِ جهازِTip sonicator لتقليص حجم هذه الجزيئات إلى 200nm عن طريقِ التحكمِ بالزمنٍ وطاقة sonicator المستخدمة.

التحاليلُ الطيفيةُ لـل FTIR أظهرت أنّ جزيئاتِ أكسيدِ الغرافين بحجميها تحتوي على أنواعٍ متعددةٍ من المجموعاتِ التي تَحوي ذرات الأكسجين موزعةً على سطحٍ جزيئاتِ أكسيدِ الغرافين. بينما أكد مجهرُ البحثِ الإلكترونيّ(SEM) والتحاليلُ الإحصائيةُ تشكلَ جزيئاتِ أكسيدِ الغرافين بحجميها. لكنَ أكسيد الغرافين بحجمه الأصغر GO-200nm كان أكثر فاعليةَ في إزالة النيكل (II) نتيجة سِعة سَطحهُ المُتَوفِر مقارنةً بأكسيدِ الغرافين GO-450nm.

ديناميكا الإدمصاصِ والعَوامِل المُتَحَكِمَة بعَمليةِ الإدمصاص كالتركيز الإبتدائيّ عند الاتزان, ودرجة الحموضة, وَدَرجِة الحَرارَة وعامِلُ الزَّمنِ وكميةُ الممتصّ فقد تَمَّ التحكمُ بها وَدِراستها باستخدامِ جِهاز الطَيف المَرئي "فوق البنفسجي" UV-visible spectroscopy. السعةُ الامتصاصيةُ لجزيئاتِ أكسيدِ الغرافين GO تزايدت بشكلٍ كبيرٍ من 45mg/g إلى 75mg/g لأكسيدِ الغرافين GO-450nm وأكسيد الغرافين GO-200nm على الترتيب, هذه النتائجُ تم الحصولُ عليها بعدَ ساعتين من التحضير.النتائجُ أظهرت احتماليةً كبيرةً بأنْ تكونَ جزيئاتُ أكسيد الغرافين GO-200nm كممتصٍ لإزالةِ أيوناتِ النيكل (II) .

Appendixes

Appendix A: Adsorption onto GO-450nm – Data Analysis

Table A - 1. pH parameter and percentage removal of Ni^{+2} ion 400 ppm adsorption on GO - 450nm, T=25 °C, t=60 min.

$[pH]$	λ_{max}	(Abs)	C_e	$(\% R)$
2	393	0.283	328.6025	17.849
4	393	0.219	254.6307	36.340
6	393	0.145	169.1102	57.725
8	393	0.138	161.0102	59.747
10	393	0.130	151.7637	62.059

Table A – 2. Percentage removal (%R) of Ni^{+2} ions 400 ppm with different doses of GO-450 nm at T=25 °C, pH=6.

Dose (mg)	Abs	λ_{max}	C_e (ppm)	%R
1	0.311	393	360.9652	9.759
2.5	0.253	393	293.9283	26.518
5	0.175	393	203.7751	49.056
10	0.145	393	169.1009	57.725
20	0.122	393	142.5173	64.371
30	0.084	393	98.5965	75.351
40	0.071	393	72.0129	79.107
60	0.056	393	66.2339	83.442
80	0.051	393	60.4548	84.886

Adsorption Isotherm Model

Table A – 3: Input data of Langmuir and freundlich isotherm models for the adsorption of Ni^{+2} at 10 min, T=25°C, pH=6.

C_i	λ_{max}	(Abs)	C_e	(% R)	q_e	C_e/q_e	ln C_e	ln q_e
200	393	0.089	104.3756	47.812	14.344	72.766	6.750	2.663
300	393	0.165	192.2171	35.928	16.167	118.895	7.561	2.783
400	393	0.244	283.5260	29.119	17.471	162.284	7.950	2.861
500	393	0.324	375.9910	24.802	18.601	202.135	8.232	2.923
600	393	0.403	467.2996	22.117	19.905	234.765	8.450	2.991
700	393	0.480	556.2969	20.529	21.555	258.083	8.624	3.071
800	393	0.560	648.7616	18.905	22.686	285.974	8.778	3.122
900	393	0.646	748.1612	16.871	22.776	328.487	8.920	3.125

Table A – 4: Input data of Langmuir and freundlich isotherm models for the adsorption of Ni^{+2} at 30 min, T=25°C, pH=6.

C_i	λ_{max}	(Abs)	C_e	(% R)	q_e	C_e/q_e	ln C_e	ln q_e
200	393	0.063	74.3245	62.838	18.851	39.427	6.611	2.937
300	393	0.111	129.8034	56.732	25.529	50.846	7.169	3.240
400	393	0.185	215.3332	46..167	27.700	77.738	7.675	3.321
500	393	0.264	306.6422	38.672	29.000	105.739	8.028	3.367
600	393	0.334	387.5488	35.409	31.868	121.611	8.262	3.462
700	393	0.418	484.6367	30.766	32.304	150.024	8.486	3.475
800	393	0.499	578.2572	27.718	33.261	173.854	8.663	3.504
900	393	0.584	676.5011	24.833	33.525	201.790	8.820	3.512

Table A – 5: Input data of Langmuir and freundlich isotherm models for the adsorption of Ni^{+2} at 60 min, T=25°C, pH=6.

C_i	λ_{max}	(Abs)	C_e	$(\% R)$	q_e	C_e/q_e	$\ln C_e$	$\ln q_e$
200	393	0.043	512.083	74.396	22.319	22.944	6.238	3.105
300	393	0.082	962.849	67.917	30.557	31.510	6.870	3.420
400	393	0.145	1691.009	57.725	34.635	48.824	7.433	3.545
500	393	0.219	2546.307	49.074	36.805	69.184	7.842	3.606
600	393	0.301	3494.071	41.765	37.589	92.955	8.159	3.627
700	393	0.381	4418.718	36.875	38.719	114.123	8.394	3.656
800	393	0.463	5366.482	32.919	39.503	135.850	8.588	3.676
900	393	0.545	6314.245	29.842	40.286	156.735	8.751	3.696

Table A – 6: Input data of Langmuir and freundlich isotherm models for the adsorption of Ni^{+2} at 90 min, T=25°C, pH=6.

C_i	λ_{max}	(Abs)	C_e	$(\% R)$	q_e	C_e/q_e	$\ln C_e$	$\ln q_e$
200	393	0.033	396.503	80.175	24.052	16.485	5.983	3.180
300	393	0.073	858.826	71.372	32.118	26.740	6.756	3.469
400	393	0.138	1610.102	59.747	35.848	44.915	7.384	3.579
500	393	0.212	2465.401	50.692	38.019	64.847	7.810	3.638
600	393	0.290	3366.932	43.884	39.496	85.247	8.122	3.685
700	393	0.370	4291.579	38.692	40.626	105.636	8.364	3.704
800	393	0.452	5239.343	34.508	41.409	126.527	8.564	3.723
900	393	0.535	6198.664	31.126	42.020	147.517	8.732	3.738

Table A – 7: Input data of Langmuir and freundlich isotherm models for the adsorption of Ni^{+2} at 120 min, T=25°C, pH=6.

C_i	λ_{max}	(Abs)	C_e	$(\% R)$	q_e	C_e/q_e	$\ln C_e$	$\ln q_e$
200	393	0.027	327.154	83.642	25.093	13.038	5.790	3.223
300	393	0.058	685.454	75.225	34.718	19.743	6.530	3.547
400	393	0.132	1540.754	61.481	36.889	41.767	7.340	3.608
500	393	0.203	2361.378	52.772	39.579	59.662	7.767	3.678
600	393	0.270	3135.770	47.737	42.963	72.988	8.051	3.760
700	393	0.352	4083.533	41.664	43.747	93.344	8.315	3.778
800	393	0.436	5054.413	36.819	44.183	114.397	8.528	3.788
900	393	0.521	6036.851	32.924	44.447	135.821	8.706	3.794

Adsorption Kinetic Model

Table A – 8: Input data of pseudo-first-order and pseudo-second-order kinetic models for the adsorption of Ni^{+2} at 200 ppm.

$Time_{min}$	λ_{max}	(Abs)	C_e	q_t	$q_e - q_t$	$ln\ q_e - q_t$	t/q_t
10	393	0.089	104.3756	14.344	10.749	2.375	0.697
30	393	0.063	74.3245	18.851	6.242	1.831	1.591
60	393	0.043	51.2083	22.319	2.774	1.020	2.688
90	393	0.033	39.6503	24.052	1.041	0.040	3.742
120	393	0.027	32.7154	25.093	0	0	4.782

Table A – 9: Input data of pseudo-first-order and pseudo-second-order kinetic models for the adsorption of Ni^{+2} at 300 ppm.

$Time_{min}$	λ_{max}	(Abs)	C_e	q_t	$q_e - q_t$	$ln\ q_e - q_t$	t/q_t
10	393	0.165	192.2171	16.167	18.551	2.921	0.619
30	393	0.111	129.8034	25.529	9.189	2.218	1.175
60	393	0.082	96.2847	30.577	4.141	1.421	1.962
90	393	0.073	85.8826	32.118	2.600	0.956	2.802
120	393	0.058	68.5454	34.718	0	0	3.456

Table A – 10: Input data of pseudo-first-order and pseudo-second-order kinetic models for the adsorption of Ni^{+2} at 400 ppm.

$Time_{min}$	λ_{max}	(Abs)	C_e	q_t	$q_e - q_t$	$ln\ q_e - q_t$	t/q_t
10	393	0.244	283.5260	17.471	19.418	2.966	0.572
30	393	0.185	215.3332	27.700	9.189	2.218	1.083
60	393	0.145	169.1009	34.635	2.254	0.813	1.732
90	393	0.138	161.0102	35.848	1.041	0.040	2.511
120	393	0.132	154.0754	36.889	0	0	3.253

Table A – 11: Input data of pseudo-first-order and pseudo-second-order kinetic models for the adsorption of Ni^{+2} at 500 ppm.

$Time_{min}$	λ_{max}	(Abs)	C_e	q_t	$q_{e-}q_t$	$ln\ q_e-q_t$	t/q_t
10	393	0.324	375.9910	18.601	20.978	3.043	0.538
30	393	0.264	306.6422	29.000	10.579	2.359	1.034
60	393	0.219	254.6307	36.805	2.774	1.020	1.630
90	393	0.212	246.5401	38.019	1.560	0.445	2.367
120	393	0.203	236.1378	39.579	0	0	3.032

Table A – 12: Input data of pseudo-first-order and pseudo-second-order kinetic models for the adsorption of Ni^{+2} at 600 ppm.

$Time_{min}$	λ_{max}	(Abs)	C_e	q_t	$q_{e-}q_t$	$ln\ q_e-q_t$	t/q_t
10	393	0.403	467.2996	19.905	23.058	3.138	0.502
30	393	0.334	387.5488	31.868	11.095	2.406	0.941
60	393	0.301	349.4071	37.589	5.374	1.682	1.569
90	393	0.290	336.6932	39.496	3.467	1.243	2.279
120	393	0.270	313.5770	42.963	0	0	2.793

Table A – 13: Input data of pseudo-first-order and pseudo-second-order kinetic models for the adsorption of Ni^{+2} at 700 ppm.

$Time_{min}$	λ_{max}	(Abs)	C_e	q_t	$q_{e-}q_t$	$ln\ q_e-q_t$	t/q_t
10	393	0.480	556.2969	21.555	22.192	3.099	0.464
30	393	0.418	484.6367	32.304	11.443	2.437	0.929
60	393	0.381	441.8718	38.719	5.028	1.615	1.549
90	393	0.370	429.1579	40.626	3.121	1.138	2.215
120	393	0.352	408.3533	43.747	0	0	2.743

Table A – 14: Input data of pseudo-first-order and pseudo-second-order kinetic models for the adsorption of Ni^{+2} at 800 ppm.

$Time_{min}$	λ_{max}	(Abs)	C_e	q_t	$q_{e-}q_t$	$\ln q_e - q_t$	t/q_t
10	393	0.646	648.7616	22.686	21.497	3.068	0.441
30	393	0.499	578.2572	33.261	10.922	2.391	0.902
60	393	0.463	536.6482	39.503	4.680	1.543	1.519
90	393	0.452	523.9343	41.409	2.774	1.020	2.173
120	393	0.436	505.4413	44.183	0	0	2.716

Table A – 15: Input data of pseudo-first-order and pseudo-second-order kinetic models for the adsorption of Ni^{+2} at 900 ppm.

$Time_{min}$	λ_{max}	(Abs)	C_e	q_t	$q_{e-}q_t$	$\ln q_e - q_t$	t/q_t
10	393	0.646	748.1612	22.776	21.671	3.076	0.439
30	393	0.584	676.5011	33.525	10.922	2.391	0.895
60	393	0.545	631.4254	40.286	4.161	1.426	1.489
90	393	0.535	619.8664	42.020	2.427	0.887	2.142
120	393	0.521	603.6851	44.447	0	0	2.699

Appendix B: Adsorption onto GO-200nm – Data Analysis

Table B - 1. pH parameter and percentage removal of Ni^{+2} ion 400 ppm adsorption on GO - 200nm at T=25 °C, t=60 min.

$[PH]$	λ_{max}	(Abs)	C_e	$(\% R)$
2	393	0.262	304.3305	23.917
4	393	0.181	210.7099	47.323
6	393	0.148	172.5683	56.858
8	393	0.128	149.4521	62.637
10	393	0.102	140.2056	64.949

Table B– 2. Percentage removal (%R) of Ni^{+2} ions 400 ppm with different doses of GO-200 nm at T=25 °C, pH=6.

Dose (mg)	Abs	λ_{max}	C_e (ppm)	%R
1	0.292	393	339.0048	15.249
2.5	0.245	393	269.6563	32.586
5	0.154	393	179.5032	55.124
10	0.109	393	127.4917	68.127
20	0.085	393	99.7523	75.062
30	0.067	393	78.9478	80.263
40	0.060	393	70.8571	82.286
60	0.051	393	60.4548	84.886
80	0.039	393	46.5851	88.354

Adsorption Isotherm Model

Table B – 3: Input data of Langmuir and freundlich isotherm models for the adsorption of Ni^{+2} onto GO-200nm at 10 min, T=25°C, pH=6.

C_i	λ_{max}	(Abs)	C_e	$(\% R)$	q_e	C_e/q_e	$ln\ C_e$	$ln\ q_e$
200	393	0.064	79.6800	60.160	18.048	44.149	6.681	2.893
300	393	0.145	172.2418	42.586	19.163	89.880	7.451	2.953
400	393	0.205	240.8062	39.798	23.879	100.844	7.787	3.173
500	393	0.290	337.9389	32.412	24.309	139.018	8.125	3.191
600	393	0.361	419.0733	30.154	27.139	154.417	8.341	3.301
700	393	0.441	510.4924	27.073	28.426	179.586	8.538	3.347
800	393	0.525	606.4824	24.189	29.028	208.930	8.710	3.368
900	393	0.601	693.3305	22.963	31.000	223.655	8.844	3.434

Table B – 4: Input data of Langmuir and freundlich isotherm models for the adsorption of Ni^{+2} onto GO-200nm at 30 min, T=25°C, pH=6.

C_i	λ_{max}	(Abs)	C_e	$(\% R)$	q_e	C_e/q_e	$ln\ C_e$	$ln\ q_e$
200	393	0.036	47.6834	76.158	22.847	20.870	6.667	3.129
300	393	0.126	150.5298	49.823	22.420	67.141	7.317	3.109
400	393	0.182	214.5232	46.369	27.822	77.106	7.671	3.326
500	393	0.261	293.3721	41.326	30.994	94.65	7.984	3.434
600	393	0.306	356.2227	40.629	36.566	97.419	8.178	3.599
700	393	0.357	414.5024	40.785	42.825	96.789	8.329	3.757
800	393	0.447	517.3488	35.331	42.398	122.023	8.551	3.747
900	393	0.524	605.3397	32.740	44.199	136.958	8.708	3.801

Table B – 5: Input data of Langmuir and freundlich isotherm models for the adsorption of Ni^{+2} onto GO-200nm at 60 min, T=25°C, pH=6.

C_i	λ_{max}	(Abs)	C_e	$(\% R)$	q_e	C_e/q_e	$\ln C_e$	$\ln q_e$
200	393	0.014	22.5431	88.728	26.618	8.469	5.418	3.282
300	393	0.120	123.1041	58.965	26.534	46.395	7.116	3.278
400	393	0.148	175.6701	56.082	33.649	52.207	7.471	3.516
500	393	0.203	238.5207	52.295	39.222	60.813	7.777	3.669
600	393	0.240	280.8020	53.199	47.879	58.648	7.940	3.869
700	393	0.319	371.0783	46.989	49.338	75.211	8.219	3.899
800	393	0.371	430.5007	46.187	55.424	77.674	8.368	4.015
900	393	0.459	531.0617	40.993	55.341	95.962	8.577	4.014

Table B – 6: Input data of Langmuir and freundlich isotherm models for the adsorption of Ni^{+2} onto GO-200nm at 90 min, T=25°C, pH=6.

C_i	λ_{max}	(Abs)	C_e	$(\% R)$	q_e	C_e/q_e	$\ln C_e$	$\ln q_e$
200	393	0.008	15.6867	92.157	27.647	5.674	5.055	3.319
300	393	0.069	85.3937	71.535	32.191	26.456	6.749	3.472
400	393	0.121	144.8161	63.795	38.278	37.833	7.278	3.645
500	393	0.182	214.5232	57.095	42.822	50.096	7.671	3.757
600	393	0.217	254.5190	57.580	51.822	49.114	7.842	3.948
700	393	0.263	307.0850	56.131	58.937	52.104	8.029	4.076
800	393	0.311	361.9364	54.758	65.709	55.082	8.194	4.185
900	393	0.436	504.7787	43.913	59.283	85.147	8.527	4.082

Table B – 7: Input data of Langmuir and freundlich isotherm models for the adsorption of Ni^{+2} onto GO-200nm at 120 min, T=25°C, pH=6.

C_i	λ_{max}	(Abs)	C_e	$(\% R)$	q_e	C_e/q_e	$\ln C_e$	$\ln q_e$
200	393	0.006	13.4012	93.299	27.989	4.788	4.898	3.332
300	393	0.052	65.9672	78.011	35.105	18.791	6.492	3.558
400	393	0.102	123.1041	69.224	41.534	29.639	7.116	3.727
500	393	0.145	172.2418	65.552	49.164	35.034	7.451	3.895
600	393	0.198	232.8070	61.199	55.079	42.268	7.753	4.009
700	393	0.201	259.0899	62.987	66.137	39.175	7.859	4.192
800	393	0.263	307.0849	61.614	73.937	41.533	8.029	4.303
900	393	0.357	414.5024	53.944	72.825	56.918	8.329	4.288

Adsorption Kinetic Model

Table B – 8: Input data of pseudo-first-order and pseudo-second-order kinetic models for the adsorption of Ni^{+2} at 200 ppm.

$Time_{min}$	λ_{max}	(Abs)	C_e	q_t	$q_{e-}q_t$	$\ln q_e - q_t$	t/q_t
10	393	0.064	79.6800	18.048	9.941	2.297	0.554
30	393	0.036	47.6834	22.847	5.142	1.637	1.313
60	393	0.014	22.5431	26.618	1.371	0.316	2.254
90	393	0.008	15.6867	27.647	0.342	-1.073	3.255
120	393	0.006	13.4012	27.989	0	0	4.287

Table B – 9: Input data of pseudo-first-order and pseudo-second-order kinetic models for the adsorption of Ni^{+2} at 300 ppm.

$Time_{min}$	λ_{max}	(Abs)	C_e	q_t	$q_{e-}q_t$	$\ln q_e - q_t$	t/q_t
10	393	0.145	172.2418	19.163	15.942	2.769	0.522
30	393	0.126	150.5298	22.420	12.685	2.540	1.338
60	393	0.120	123.1041	26.534	8.571	2.148	2.261
90	393	0.069	85.3937	32.191	2.914	1.069	2.796
120	393	0.052	65.9672	35.105	0	0	3.418

Table B – 10: Input data of pseudo-first-order and pseudo-second-order kinetic models for the adsorption of Ni^{+2} at 400 ppm.

$Time_{min}$	λ_{max}	(Abs)	C_e	q_t	$q_{e-}q_t$	$\ln q_e - q_t$	t/q_t
10	393	0.205	240.8062	23.879	17.655	2.871	0.419
30	393	0.182	214.5232	27.822	13.712	2.618	1.078
60	393	0.148	175.6701	33.649	7.885	2.065	1.783
90	393	0.121	144.8161	38.278	3.256	1.180	2.351
120	393	0.102	123.1041	41.534	0	0	2.889

Table B – 11: Input data of pseudo-first-order and pseudo-second-order kinetic models for the adsorption of Ni^{+2} at 500 ppm.

$Time_{min}$	λ_{max}	(Abs)	C_e	q_t	$q_{e-}q_t$	$\ln q_e - q_t$	t/q_t
10	393	0.290	337.9389	24.309	24.855	3.213	0.411
30	393	0.261	293.3721	30.994	18.170	2.899	0.968
60	393	0.203	238.5207	39.222	9.942	2.296	1.529
90	393	0.182	214.5232	42.822	6.342	1.847	2.102
120	393	0.145	172.2418	49.164	0	0	2.441

Table B – 12: Input data of pseudo-first-order and pseudo-second-order kinetic models for the adsorption of Ni^{+2} at 600 ppm.

$Time_{min}$	λ_{max}	(Abs)	C_e	q_t	$q_{e-}q_t$	$\ln q_e - q_t$	t/q_t
10	393	0.361	419.0733	27.139	27.940	3.330	0.368
30	393	0.306	356.2227	36.566	18.513	2.918	0.820
60	393	0.240	280.8020	47.879	7.200	1.974	1.253
90	393	0.217	254.5190	51.822	3.257	1.181	1.737
120	393	0.198	232.8070	55.079	0	0	2.179

Table B – 13: Input data of pseudo-first-order and pseudo-second-order kinetic models for the adsorption of Ni^{+2} at 700 ppm.

$Time_{min}$	λ_{max}	(Abs)	C_e	q_t	$q_{e-}q_t$	$\ln q_e - q_t$	t/q_t
10	393	0.441	510.4924	28.426	37.711	3.630	0.352
30	393	0.357	414.5024	42.825	23.312	3.149	0.701
60	393	0.319	371.0783	49.338	16.799	2.821	1.216
90	393	0.263	307.0850	58.937	7.200	1.974	1.527
120	393	0.201	259.0899	66.137	0	0	1.814

Table B – 14: Input data of pseudo-first-order and pseudo-second-order kinetic models for the adsorption of Ni^{+2} at 800 ppm.

$Time_{min}$	λ_{max}	(Abs)	C_e	q_t	$q_{e-}q_t$	$ln\ q_e-q_t$	t/q_t
10	393	0.525	606.4824	29.028	44.909	3.805	0.344
30	393	0.447	517.3488	42.398	31.539	3.451	0.708
60	393	0.371	430.5007	55.424	18.513	2.918	1.083
90	393	0.311	361.9364	65.709	8.228	2.108	1.369
120	393	0.263	307.0849	73.937	0	0	1.623

Table B – 15: Input data of pseudo-first-order and pseudo-second-order kinetic models for the adsorption of Ni^{+2} at 900 ppm.

$Time_{min}$	λ_{max}	(Abs)	C_e	q_t	$q_{e-}q_t$	$ln\ q_e-q_t$	t/q_t
10	393	0.601	693.3305	31.000	41.825	3.733	0.323
30	393	0.524	605.3397	44.199	28.626	3.354	0.679
60	393	0.459	531.0617	55.341	17.848	2.861	1.084
90	393	0.436	504.7787	59.283	13.542	2.606	1.518
120	393	0.357	414.5024	72.825	0	0	1.648